UNIVERSITÀ DI PISA

DIPARTIMENTO DI INGEGNERIA MECCANICA, NUCLEARE E DELLA PRODUZIONE

EX-VESSEL BREAK IN THE ITER DIVERTOR COOLING LOOP USING THE ECART CODE

S. Paci

DIMNP 036 (04)

Work performed for ENEA Thermonuclear Fusion Division in the framework of the Research Contract No. 04/58/28/AA (Prot. ENEA/2004/23994/FUS-STG)

SUMMARY

In the present report DIMNP 036 (04) the detailed description of the task carried out by the DIMNP of Pisa University for ENEA-CR Frascati (Rome) in the framework of the Research Contract No. 04/58/28/AA (Prot. ENEA/2004/23994/FUS-STG) is presented. This work is related to the application of the CESI and Edf ECART code on the analysis of a large ex-vessel break in the divertor cooling loop of the ITER reactor. These activities are carried out in the general framework of the validation phase of the ECART code, initially developed by ENEL and EdF for integrated analysis of severe accidents in LWRs, for its application on incidental sequences related to the ITER fusion plant.

ECART was originally designed and validated for traditional NPP safety analyses and it is internationally recognized as a relevant nuclear source term code for nuclear fission plants. It permits the simulation of chemical reactions and transport of radioactive gases and aerosols under two-phase flow transients in generic flow systems, using a built-in thermal-hydraulic model.

A comparison of the ECART data with the results obtained by NFR Studsvik Nuclear AB (Nyköping, Sweden), utilising the MELCOR code in its fusion version for the same sequence, has been also performed during the present task. This comparison gives a quite good qualitative and quantitative agreement in the results, both for the thermal-hydraulics main parameters and the environmental radioactive releases.

INDEX

Index of Tables

Index of Figures

Acronyms

ACP	Activated Corrosion Product
AMMD	Aerosol Mass Median Diameter
AV	Aerosol and Vapour ECART module
CFC	Carbon Fibre Composite
CH	Chemical ECART module
DIV	Divertor
DT	Drain Tank
DV	Divertor
EDS	Emergency Detritiation System
EFDA	European Fusion Development Agreement
EU	European Union
FPSS	Fast Plasma Shutdown System
FW/BL	First Wall/Blanket
GSD	Geometric Standard Deviation
GSSR	ITER Generic Site Safety Report
HTS	Heat Transport System
HVAC	Heat, Ventilation and Air Conditioning system
HX	Heat Exchanger
ITER	International Thermonuclear Experimental Reactor
LOCA	Loss Of Coolant Accident
LOVA	Loss Of Vacuum Accident
LWR	Light Water Reactor
LIM	Limiter
MMD	Mass Median Diameter
N-VDS	Normal Vent Detritiation System
NB	Neutral Beam
NBI	Neutral Bean Injector
NPP	Nuclear Power Plant
PFC	Plasma Facing Component
PHTS	Primary Heat Transport System
PSS	Pressure Suppression System
QA	Quality Assurance
RR	Reaction Rate
SA	Severe Accident
ST	Suppression Tank
ST-VS	Suppression Tank Venting System
STP	Standard Temperature and Pressure
S-VDS	Stand-by Vent Detritiation System
TCWS	Tokamak Cooling Water System
TH	Thermal-hydraulic ECART module
VV	Vacuum Vessel
VVPSS	Vacuum Vessel Pressure Suppression System

Control Volume Nomenclature

BROK	diagnostic duct
COOLI	Cooling Loop Inlet Pipes
COOLO	Cooling Loop Outlet Pipes
DBLEED	Bleed lines towards Drain Tank
DRTANK	Drain Tank
EMDETS	Emergency Detritiation System (towards VV)
ExtCln	inleakage in GRNR and in PITVOL from the environment
ExtDet	exhausted detritiation system S-VDS towards the environment
ExtDev	detritiation system from VV towards the environment
Extern	releases towards Environment from Vault (no filtered)
ExterP	releases towards Environment from PITVOL (no filtered)
ExtHVA	Releases from Vault through HVAC
ExtPSS	Releases from ST VS
ExtVnt	from generic & PIT room towards environment after 30 s from the accident
GENR	generic room
OPIPE1	duct outlet from vault in the first 30 s of the accident H-VAC
PITVOL	Pit volume
RDPIPE	Rupture Disk Pipe towards PSS Tank
SBYVDS	Ventilation Detritiation System S-VDS
VAULT	Upper TCWS Vault
VAULTL	Lower TCWS Vault
VACV	Vacuum Vessel
VVPSSY	Vacuum Vessel Pressure Suppression System
VVPSSV	PSS Venting System ST VS

1. INTRODUCTION

In the present Report the detailed description of the task carried out by the Department of Mechanical, Nuclear and Production Engineering (DIMNP) of the UNIVERSITÀ DI PISA for the ENEA Frascati (Rome) in the framework of the Research Contract **No. 04/58/28/AA (Prot. ENEA/2004/23994/FUS-STG)** is presented. This work is related to the application of the ENEL (now CESI[1]) and EdF ECART (ENEL Code for Analysis of Radionuclide Transport) code [Parozzi, 1997a and 1997b] on a large ex-vessel break in the ITER divertor cooling loop and in the comparison of the ECART code results with the data obtained by Studsvik Nuclear AB (S) for the same ITER LOCA sequence [Sheng, 2003] but employing the MELCOR code in its fusion version, for the Quality Assurance of these safety studies.

All the related geometrical data for the plant nodalisation with ECART and the specific initially and boundary conditions for the different calculations have been furnished to the DIMNP by ENEA Frascati Fusion Division at the beginning of the present work while the ECART code was made available to the Pisa University and ENEA FUS by CESI Milan. The main reference documentation for the presented ECART analyses is constituted by the following 4 reports in order of priority (it is necessary to immediately highlight as, to allow a better comparison with the MELCOR results, the different assumptions from the SADL data present in the MELCOR analyses have been also maintained in the ECART model):

1) ChunHong Sheng, Lise-Lotte Spontón, *"ITER Divertor Ex-Vessel Pipe Break"*, Studsvik Nuclear, N(R)-03/075, December 15, 2003 and the related input and output files for MELCOR.

2) H.W. Bartels et alii, *"Safety Analysis Data List - 4 (SADL-4)"*. Version 4.0.2. August 19, 2003.

3) H.W. Bartels, *"Accident Analysis Specification (AAS)"*, Version 4.beta.1, August 2003.

4) L. Topilski, *"Consequences of large ex-vessel and in-vessel coolant breaks in the divertor cooling loop with different models of air bypass"*, G 84 RI 23 04-06-15 R 0.1 June 15, 2004.

[1] CESI acquired at the end of 1999 the Research & Development division of ENEL.

Historically, in the frame of the Generic Site Safety Report GSSR for the ITER experimental plant (Figure 1.1), several accident analyses have been carried out [GSSR, 2001], [Cambi, 2003] to quantify in detail the radiological risk linked with the possible releases to the external environment of radioactive materials. In this context the hypothetical double-ended pipe rupture outside the VV of the largest pipe of the DV cooling circuit was analysed to bound all possible leaks in the ex-vessel section of a divertor primary heat transfer system during the pulse operation. However, both the plant and the sequence data employed for these new ECART and MELCOR analyses differ from the previous ones employed for the GSSR studies [GSSR, 2001] and for a previous ECART verification analysis [Cambi, 2003], as will be in detail outlined in the following of the present report.

All these activities have been carried out in the general framework of the developed and validation phase [Paci, 2004 b] of the ECART code, initially developed by ENEL and EdF for integrated analysis of SAs in LWRs [Wright, 1994], for its application on incidental sequences related to the ITER fusion plant. Main points of this validation activity were, in the recent past, the activities related on the Japanese ICE facility for the thermal-hydraulics of the ITER PSS [Paci, 2004 a] and on the ENEA STARDUST experimental apparatus on dust resuspension inside the VV [Forgione, 2004].

Historically, the use of this computational tool for the safety analyses of tokamak-type fusion reactors started in 1996 through a scientific cooperation among DIMNP, ENEL and ENEA Nuclear Fusion Division, in the framework of the EFDA Agreement. The interesting possibility offered by ECART to perform integrated accident sequence analyses, up to the environmental releases, avoiding complex interfaces between thermal-hydraulics and transport models or between circuit and containment codes, was a basic reason for this interest. Through an “ad-hoc” contract between ENEA and ENEL Research, the chemical data bank of ECART was for these reasons updated and new models for the oxidation reactions between air or steam and beryllium, tungsten and graphite walls and dust were included [Parozzi, 2000].

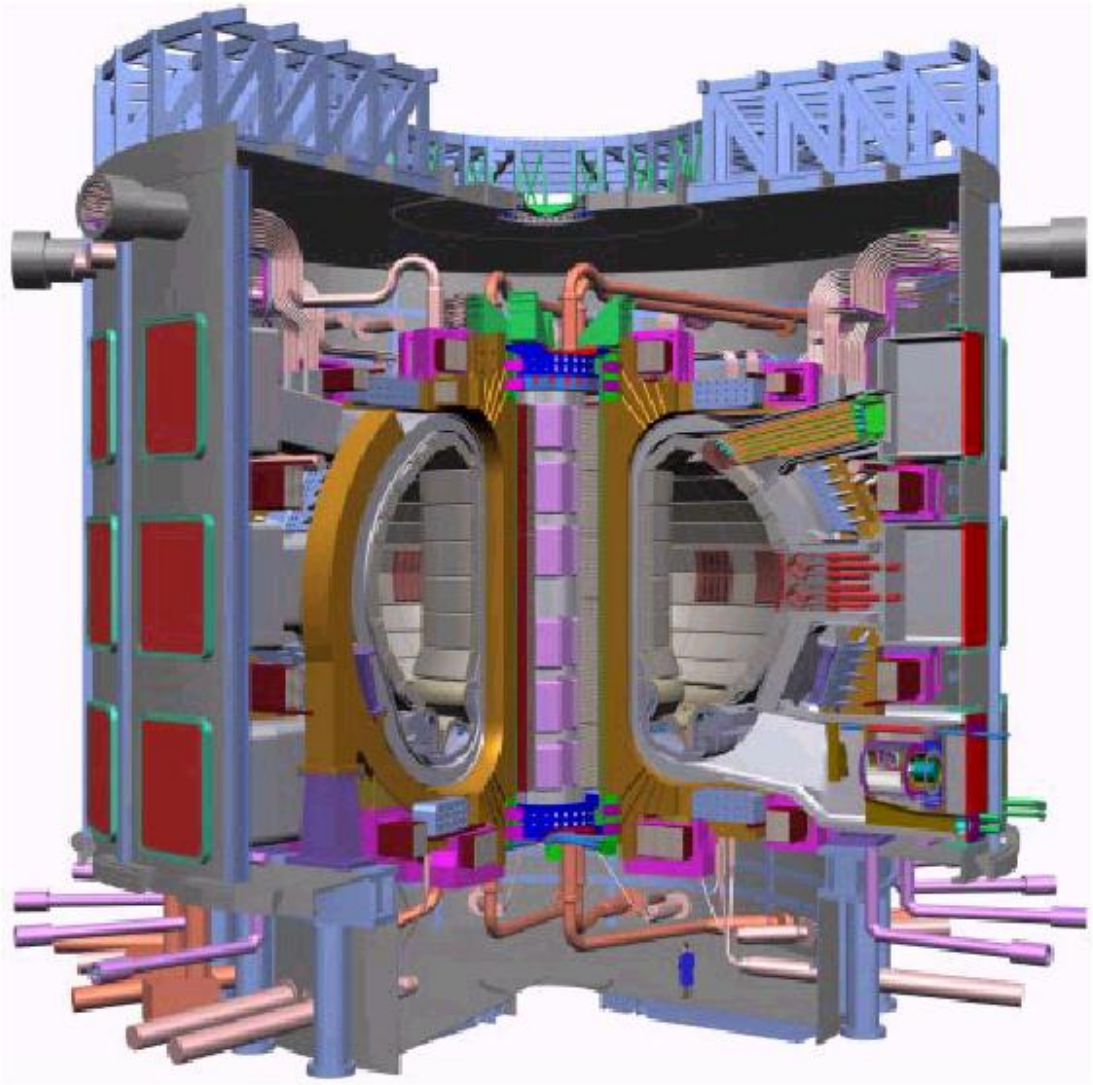

Figure 1.1: Schematic of the basic device of ITER.

2. OVERVIEW OF ECART MODELS

2.1 Main Features of the Code

ECART is designed [Parozzi, 1997a and 1997b] to operate with three sections (Figure 2.1), linked together, but able to be activated also as stand-alone modules:

1. **thermal-hydraulic (th)-** providing boundary conditions for chemistry and aerosol/vapour transport models;
2. **aerosol and vapour (av)-** calculating the amount of radioactive or toxic substances that may be retained or released in the analyzed circuit components;
3. **chemical (ch)** section - chemical equilibrium among the compounds (only in vapour form) and reactions between gaseous phase and solid materials.

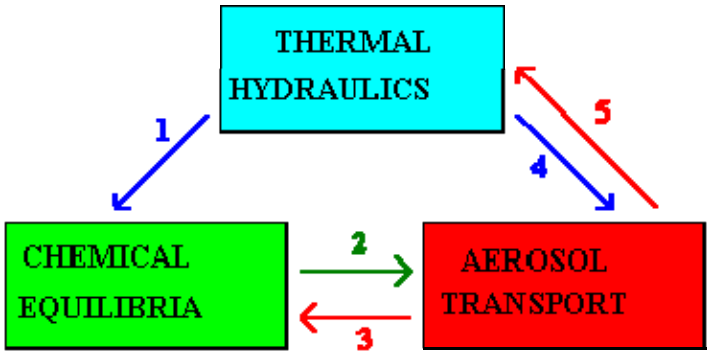

Figure 2.1: Schematic of the linking among the three main sections of the ECART code.

1. *thermal-hydraulic boundary conditions for chemical reactions;*
2. *quantity of each chemical compound in gaseous phase;*
3. *concentration of airborne reactants;*
4. *thermal-hydraulic boundary conditions for aerosol and vapours transport phenomena;*
5. *heat sources associated to transported species (i.e., radioactive decay), and aerosol concentrations capable to modify gas physical properties.*

The code applies to pure transport phenomenology (mass, energy, momentum transfer and physico-chemical processes) in whatever part of a given circuit. Support by other tools or experimental data can be used as boundary conditions or to account plant-dependent phenomena (e.g. releases from fuel, intervention of specific devices, etc.). The ECART structure is designed to treat the thermal-

hydraulic phenomena and the aerosol/vapour transport in an arbitrary flow system that the user can arbitrarily subdivide into a series of control volumes connected by flow junctions, chosen on the basis of considerations regarding geometrical features, thermal-hydraulic conditions or the expected retention of aerosols and vapours. Other details of transport analysis can be also decided by the user, like the number of chemical species, the number of aerosol size discretization bins, the occurrence of agglomeration and the multicomponent description.

Inside each control volume, a *two-region model* is adopted (Figure 2.2), being the liquid pool separated from the atmosphere. Within each region, thermal equilibrium is always assumed. Therefore, non-equilibrium effects related to superheated vapour injected in the pool or subcooled water sprayed in the atmosphere are separately accounted for.

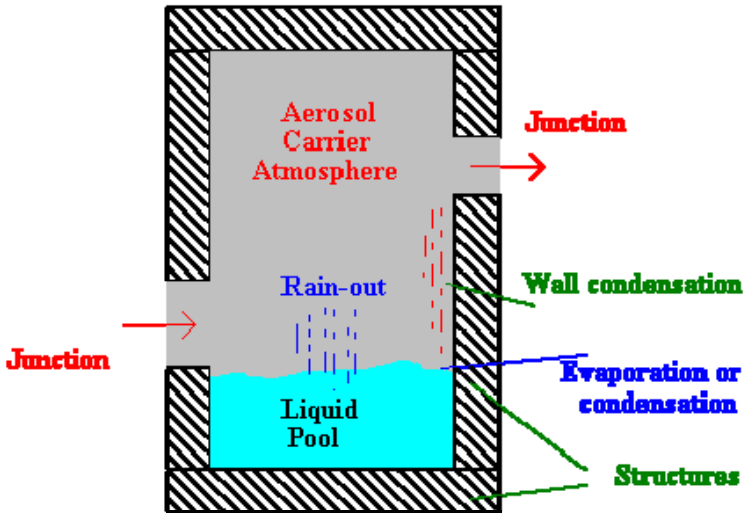

Figure 2.2: Control volume model adopted for ECART thermal-hydraulics.

Aerosols are assumed to be *well-mixed* inside the volumes. This assumption requires that the amount of vapour and/or aerosol removed within the control volume is “small” in relation to the total amount of material transported throughout the control volume itself. A corrective action (called “*plug*” flow) is provided for those volumes, like long pipes, having only a radial mixing (a concentration gradient exists along the pipe). The direction and the rate of the carrier flow can be directly assigned in input, together with other boundary data, or can be predicted by the thermal-hydraulic section. The direction can change with time, although the aerosol transport through junctions is treated as one-dimensional (i.e. there is not simultaneous mixing through a junction).

Two-dimensional flows, required to simulate scenarios where the natural convection streams could enhance the mixing among the volumes, can be accounted using two junctions to describe the exchanges between two volumes. Recirculation phenomena or chimney-effects promoted by injection of hot or lighter gas into large environments are taken into account by aerosol models, in the absence of any sub-nodalisation, through the estimate of a "recirculation velocity".

2.1.1 Thermal-Hydraulic Models

Basing on previous DIMNP experience in the development & application of models for analyzing the thermal-hydraulics during postulated accidents and considering the peculiarities of the av models, the following characteristics were established for the th section:

- capability of describing th accident transients in NPP circuits, with the degree of detail required by the av section, and capability of processing incomplete experimental data providing the lacking information on local behaviour;
- transport simulation of the aerosol carrier gases expected within LWR plants under SA conditions and usually employed in experimental tests (steam, argon, helium, hydrogen, carbon dioxide, carbon monoxide, krypton, nitrogen, oxygen and xenon);
- solution of mass, energy and momentum balance equations in order to provide for realistic representations of fluid flow and heat transfer;
- calculation of pool levels in the control volumes and evaluation of steam suppression effects to support the aerosol scrubbing phenomenology;
- steam condensation modelled by splitting bulk and wall condensation (influencing, respectively, aerosol growth and aerosol diffusiophoretic deposition);
- allowance for counter-current flow conditions at junctions;
- capability of evaluating wall heat transfer taking into account wall thermal conductivity changes due to aerosol deposition and radioactive decay heat sources;
- possibility of characterizing heat structure surfaces with local hydraulic parameters having strong influence on aerosol deposition and resuspension mechanisms (i.e. hydraulic diameter, local fluid velocity and Reynolds number, etc.);
- capability to analyze both containment and PS scenarios.

The assumption of complete stratification in a control volume is fairly well suited for containment analyses. It has some limitations in pipelines, but these limitations are accepted considering that, under SA conditions, single-phase flow (superheated steam-hydrogen mixture) or stratified flow (formation of water sumps in cold components) is likely to occur. A complete solution of the problem would require flow regime maps and constitutive laws for interfacial area and heat transfer under the various regimes. However, this kind of accident scenarios, expected to be of minor importance in terms of ST (e.g., SG tube rupture), would imply removal mechanisms differing from those mainly influencing the ST associated to the SAs normally considered for probabilistic safety assessments.

2.1.2 Aerosol and Vapour Models

Although ECART adopts the classic well-mixed assumption to describe the transport within each control volume, the deposition and resuspension phenomena can be described by dividing each control volume into sub-regions (normally, coincident with single heat structures or sumps), where local thermal-hydraulic conditions (temperature, gas flow velocity, etc.) can be taken into account. This way, small components or devices can be analyzed as part of larger control volumes, with a unique run of the master aerosol equation and longer time steps. Within each control volume, all phenomena that can be responsible for retention or re-entrance of radioactive or toxic substances can be taken into account (Figure 2.3).

Transport of volatile substances

Because of their negligible latent heat, condensation and evaporation of volatile species onto and from airborne particles and structure surfaces are dynamically calculated by diffusion equations. Conversely, steam-water phase changes can be either calculated by the th module or assigned as input. The condensation and evaporation onto and from airborne particles promotes aerosol growth or shrinkage, modify the two shape factors if necessary (see next paragraph) while the presence of a liquid phase in an aerosol deposit can inhibit its resuspension. Irreversible sorption of CsOH, I, I_2, HI, Te and Te_2 vapours onto wall surfaces (made by stainless steel or nickel alloys) and airborne particles is also modelled by adopting experimentally based correlations [Parozzi, 1997b].

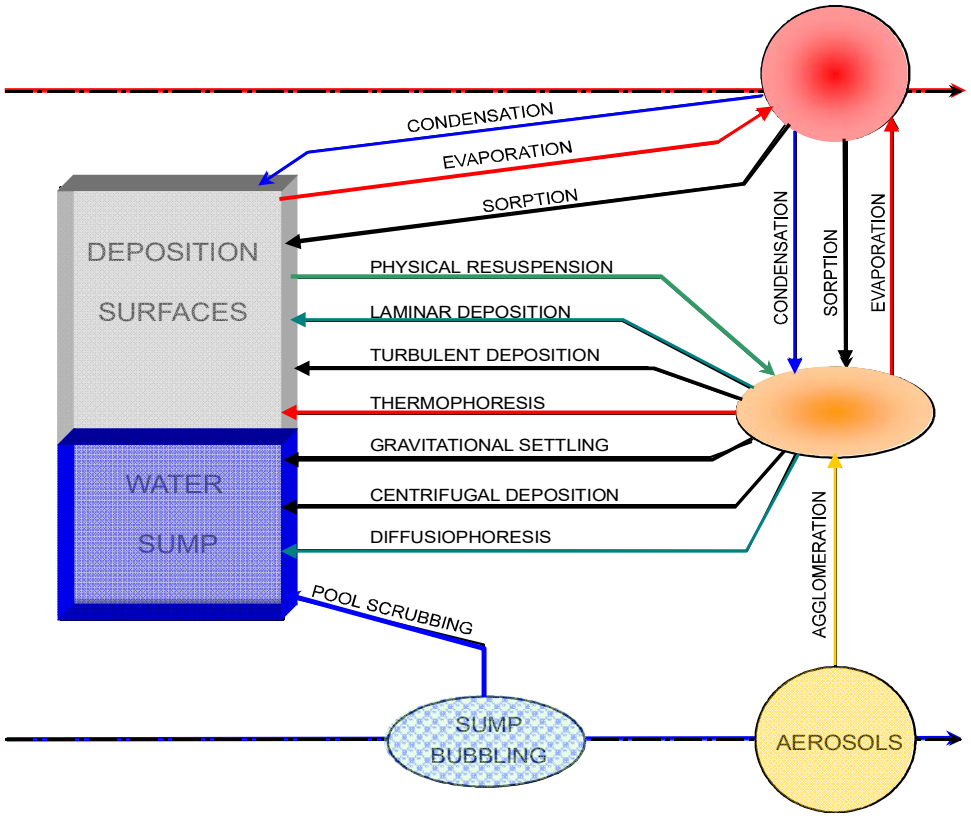

Figure 2.3: Aerosol and vapour transport phenomena simulated in each control volume.

Transport of aerosol particles

ECART works with discretised size distributions (Figure 2.4) both for airborne and deposited particles and the number of size bins is an input choice (default 20). Ordinary differential equations solvers with implicit integration methods allow saving computing time and preventing numerical instabilities. To compute the evolution of aerosol particles, mono-component basic aerosol equations can be used as default choice (i.e., at a given time, all the size bins in a given volume have the same composition). A multicomponent description of both airborne and deposited particles is possible optionally. This multicomponent approach (i.e., each size bin has its own composition), is obtained through an approximation: the av module individually tracks the transported species in each size bin, accounting for sources, particle growths or shrinking, depositions, resuspensions, etc.. The correctness and the stability of this multicomponent approach were tested through virtual tests having a known solution.

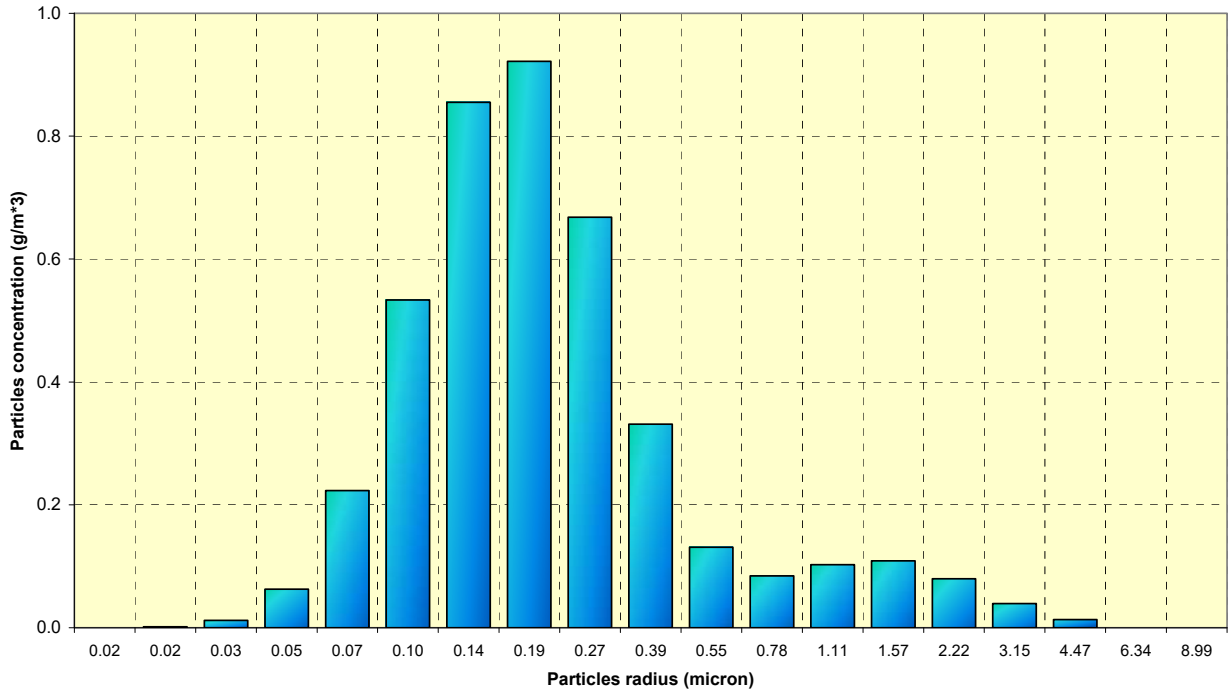

Figure 2.4: Aerosol particle size distribution modelled by ECART at a given time.

Asphericity of aerosol particles is simulated by input assigning two size-dependent shape factors:

- '*aerodynamic shape factor'* χ, accounting for different resistance to motion of the actual particles if compared to the mass-equivalent sphere;
- '*collision shape factor'*γ, accounting for the increased effective collision cross-section.

The spherical shape is the code default for the particles (χ = 1.0 and γ = 1.0) but larger values are normally present in a RCS for "*dry*" particles [Brockmann 1985]. This spherical shape is always assumed for "*wet*" particles, having an input given mass fraction of water (default 0.7).

The agglomeration models are based on the calculation of "*collision kernels*" related to the different mechanisms for agglomeration of the airborne particles. The collision frequency is then calculated multiplying this kernel by the aerosol concentration. Three processes of agglomeration are taken into account:

1. Brownian (formula derived by Smoluchowski);
2. Gravitational (collision between particles having different settling velocities);
3. Turbulent, shear and inertial (Saffman and Turner's formula).

Particle growth due to bulk condensation of vapours and steam is modelled, also allowing the simulation of possible hygroscopic behaviour of particles through the Van't Hoff factor characterising the hygroscopicity of the considered species. The Kelvin effect is taken into account in the case of steam condensation, which is inhibited for particles having radii smaller than the critical radius calculated by the code.

The deposition of aerosol particles onto surfaces is calculated as the sum of "deposition velocities" attributed to different effects:

- inertial impaction from turbulent flow (according to Liu-Agarwal observations);
- diffusion from turbulent flow (Davies' formula);
- diffusion from laminar flow (Gormley-Kennedy's formula);
- thermophoresis (Brock's correlation with Talbot's coefficients);
- gravitational settling (Stokesian and non-Stokesian regimes);
- centrifugation in curved pathways and pipe bends (Stokesian and non-Stokesian regimes; trapping in narrow bends);
- diffusiophoresis (Schmitt-Waldmann's formula).

The particle resuspension and the inhibition of their deposition caused by fast gas flows is evaluated though a semi-empirical approach based on a relationship between the acting forces (adhesive and aerodynamic) and resuspension rates experimentally measured. The model accounts for the transient resuspension of already formed deposits and the steady-state resuspension occurring in equilibrium with particle turbulent deposition.

In water sumps, the particle scrubbing is modelled accounting for aerosol phenomena occurring within the rising bubbles: inward and condensing steam, gravitational settling, particle diffusion and centrifugation. The evolution of bubbles (growth, asphericity, break-up and rise velocity) is simulated on the basis of experimental data and in agreement with the boundary conditions provided by thermal-hydraulics.

Coupling between aerosol and thermal-hydraulic calculations

In the case of a coupled run of aerosols and thermal-hydraulics, the av section receives all the required data from th, and gives a feedback to the heat and mass transfer calculations. Then, the influence of high airborne aerosol concentrations on the gas physical properties (apparent density and viscosity) is taken into account. Decay heat can be accounted for the most powerful elements undergoing transport processes (Kr, Rb, Sr, Mo, Ru, Ag, Sn, Sb, Te, I, Xe, Cs and Ba) through time-dependent β and γ specific power correlations.

The coupling among the two sections is explicit: as the th section and the av section are advanced with their own convergence criteria, a proper logic of time step synchronization is adopted. The thermal-hydraulic problem is firstly solved over the time interval between two synchronous conditions (of the order of the lowest Courant limit in the nodalisation), often adopting short time steps, suitable for numerical explicit algorithms. The aerosol calculations follow, with implicit integration methods allowing time steps usually an order of magnitude longer than the thermal-hydraulics ones: this technique gives the possibility to smooth out the data related to flow rates and pressures calculated by the th section in the case of oscillations due to limited instabilities.

2.1.3 Chemistry Models

The ch section provides the av section with the gaseous phase composition on the basis of equilibrium conditions. The chemical equilibrium calculation occurs whenever significant changes in temperatures, pressures or vapour species amount are calculated by the other two sections. Possible phase changes causing condensation onto walls and airborne particles, however, are dynamically accounted for in the diffusive model employed by the av section.

The solving algorithm is based on Gibbs free energy minimization at constant pressure and temperature of the system: this allows the calculation of the equilibrium composition of the mixture in terms of molar fractions. In order to manage the formation and evolution of radionuclide species within LWR RCSs, this ch section is dimensioned for environments characterized by temperatures in the range from room conditions up to 2,500. K, with pressures up to 15. MPa. Real gas behaviour is modelled by fugacity coefficients computed according to Redlich-Kwong-Soave equation for a hydrogen-steam mixture. The code uses a non-linear minimization algorithm preventing the linearization of the function to be minimized, which would affect the correctness of final results.

The possible reactants and reaction products considered (Table 2.1) are the carrier gas components, with the exception of nitrogen and noble gases, and most of the species which can be transported in form of vapours. To match with the phase changes calculated by the av section, super saturation conditions of the predicted vapours are accepted by chemistry algorithms. The databases contained in chemical section are also used to determine the temperature-dependent saturation pressures of all volatile species. The ch section contains information about the most representative compounds for a LWR SA sequence. Further compounds, involved in fusion reactor safety problems, are also included in the catalogue (Table 2.1) as discussed in the next paragraph.

Table 2.1: Catalogue of the chemical species available in ECART

Species name	Species description	Normal melting point [K]	Normal boiling point [K]	Solid density [kg/m^3]	Liquid density [kg/m^3]	Evap./ cond.	Chemistry
Ag	silver	1234	2436	10500	9320	yes	yes
AgI	silver iodide	831	1779.	5683	4830	yes	yes
B	boron	2350	4139	2355	2080	yes	yes
BI3	boron triiodide	323	483	3350	3350	no	yes
B2O3	boron sesquioxide	723	2133	2460	2090	yes	yes
Ba	barium	1000	2119	3510	3081	yes	yes
BaI	barium monoiodide	--	--	--	--	no	yes
BaI2	barium iodide	984	2337	5150	4380	yes	yes
BaO	barium oxide	2286	--	5720	4862	yes	yes
BaOH	barium hydroxide	--	--	--	--	no	yes
Ba(OH)2	barium dihydroxide	681	1325	2180	1850	yes	yes
Be	beryllium	1560	2741	1850	1500	yes	yes(3)
BeO	beryllium oxide	2821	--	3010	2558	no	yes(3)
C	carbon	3925	5100	2250	1912	no	yes(3)
Cd	cadmium	594	1038	8642	7530	yes	yes
CdI	cadmium monoiodide	--	--	--	--	no	yes
CdI2	cadmium diiodide	660	1069	5670	4820	yes	yes
CdO	cadmium oxide	--	--	6950	5900	yes	yes
Cd(OH)2	cadmium dihydroxide	--	--	4790	4070	no	yes
CdTe	cadmium telluride	1314	--	6200	5270	no	yes
CH4	methane	--	--	--	--	no	yes
Co	cobalt	1768	3198	8900	7670	yes	yes
Cr	chromium	2130	2945	7200	6460	yes	yes
CrI	chromium monoiodide	--	--	--	--	no	yes
CrI2	chromium diiodide	1129	--	5196	4417	yes	yes
CrO	chromium oxide	--	--	--	--	no	yes
Cr2O3	chromium sesquioxide	2603	4273.	5210	4430	no	yes
Cs	cesium	301.5	948	1878	1468	yes	yes
CsBO2	cesium borate	--	--	--	--	no	yes
CsI	cesium iodide	900	1553	4510	4057	yes	yes
CsO	cesium monoxide	--	--	--	--	no	yes
CsOH	cesium hydroxide	500	1263	3675	3308	yes	yes(1)
Cs2	diatomic cesium	--	--	--	--	no	yes
Cs2CrO4	cesium chromate	--	--	4237	4237	no	yes
Cs2MoO4	cesium molybdate	-	-	1000	0850	yes	yes
Cs2O	cesium oxide	763	763	4250	3610	yes	yes
Cs2(OH)2	cesium dihydroxide	--	--	--	--	no	yes
Cs2Te	cesium telluride	--	--	--	--	no	yes
Cs2TeO3	cesium tellurite	--	--	1000	0850	no	yes
Cs2ZrO3	cesium zirconate	--	--	1000	0850	no	yes
Cu	copper	1358	2843	8920	7950	yes	yes
CuO	copper monoxide	1599	2073	6400	5440	yes	yes
D	elemental deuterium	--	--	--	--	no	yes
D2	molecular deuterium	--	--	--	--	no	yes
Fe	iron	1809	3132	7860	7020	yes	Yes(2)
FeI2	iron iodide	-	-	5320	4522	yes	yes
FeO	iron oxide	1650	3687	5700	4840	yes	yes
Fe2I4	iron iodide	--	--	--	--	no	yes
Fe2NiO4	diiron nickel tetraoxide	--	--	??	--	no	yes

Fe2O3	iron sesquioxide	1838.	--	5240	4450	no	yes
Fe3O4	iron tetraoxide	1870	--	5180	4400	no	yes
H	Elemental hydrogen	--	--	--	--	no	yes
HBO2	boric acid	--	--	--	--	no	yes
HI	hydrogen iodide	--	--	--	--	no	yes
H2O	water	273	373	1000	1000	yes	no
H2Te	hydrogen telluride	--	--	--	--	no	yes
H3BO3	boric acid	--	--	--	--	no	yes
I	elemental iodine	--	--	--	--	no	Yes(1)
I2	molecular iodine	387	458	4930	4930	yes	yes(1)
In	indium	430	2353	7300	5585	yes	yes
InI	indium monoiodide	624	986	5310	4514	yes	yes
InTe	indium telluride	342	--	6290	6290	no	yes
In2O	indium suboxide	--	--	--	--	no	yes
In2O3	indium sesquioxide	--	--	7179	6100	no	yes
In2Te	diindium telluride	--	--	--	--	no	yes
Li2O	lithium oxide	1843	2836	2013	1711	yes	yes
LiOH	lithium hydroxide	744	1897	1460	1241	yes	yes
Mn	manganese	1517	2332	7200	6430	yes	yes
MnI2	manganese diiodide	911	--	5000	4250	no	yes
MnO	manganese oxide	2115	--	5445	4630	no	yes
Mn2O3	manganese sesquioxide	--	--	4500	3820	no	yes
Mn3O4	trimanganese tetraoxide	1835	--	4856	4130	no	yes
Mo	Molybdenum	--	5833	10200	8670	yes	yes
MoO2	molybdenum dioxide	--	--	6470	5500	yes	yes
MoO3	molybdenum trioxide	1075	1428	4692	3988	yes	yes
Ni	nickel	1726	3005	8900	7780	yes	yes(2)
Ni(CO)4	nickel carbonyl	248	316	1320	1320	no	yes
NiI2	nickel iodide	1070	--	5834	4960	no	yes
NiO	nickel monooxide	2263	--	6670	5700	yes	yes
O	elemental oxygen	--	--	--	--	no	yes
OH	hydroxil	--	--	--	--	no	yes
RbI	rubidium iodide	929	--	3550	2870	yes	yes
RbOH	rubidium hydroxide	574	--	3203	2723	no	yes
Ru	ruthenium	2523	4173	12300	10900	yes	yes
RuO2	ruthenium dioxide	--	--	6970	5920	no	yes
RuO3	ruthenium trioxide	--	--	--	--	no	yes
Sb	antimony	904	2023	6684	5681	yes	yes
SbTe	antimony monotelluride	--	--	--	--	no	yes
Sb2	diatomic antimony	--	--	-	-	no	yes
Sb2O3	antimony trioxide	939	1823	5670	4820	no	yes
Sb2Te3	antimony tritelluride	902	--	6500	5525	no	yes
Sb4	tetraatomic antimony	--	--	--	--	no	yes
Sn	tin	505	2873	7280	7000	yes	yes
SnH4	tin tetrahydride	--	--	--	--	no	yes
SnI2	tin iodide	593	990	5290	4497	yes	yes
SnO	tin monoxide	--	--	6446	5448	yes	yes
SnO2	tin dioxide	1400	2073	6950	5910	no	yes
SnTe	tin monotelluride	1079	--	6480	5510	yes	yes
Sr	strontium	1050	1685	2600	2210	yes	yes
SrI2	strontium iodide	811	2178	4549	3870	yes	yes
SrO	strontium oxide	2938	3273	4700	3990	no	yes
SrOH	strontium hydroxide	--	--	--	--	no	yes
Sr(OH)2	Strontium dihydroxide	783	1017	3625	3080	yes	yes
T	Elemental tritium	--	--	--	--	no	yes
T2	moleculat tritium	--	--	--	--	no	yes

Te	tellurium	723	1327	6250	5489	yes	yes(1)
TeO2	tellurium dioxide	1006	1518	5790	4920	yes	yes
Te2	diatomic tellurium	--	--	--	--	no	yes(1)
U	uranium	--	4091	19050	16190	yes	yes
UO2	Uranium dioxide	3120	--	10960	9320	yes	yes
W	Tungsten	3680	5931	19350	17600	yes	yes(3)
WO3	tungsten trioxide	1745	2110	7160	6086	yes	yes(3)
Zn	zinc	693	1179	7140	6570	yes	yes
ZnO	zinc oxide	2248	--	5606	4770	no	yes
Zr	zirconium	--	3851	6490	5516	yes	yes
ZrI4	zirconium tetraiodide	772	--	1000	1000	yes	yes
ZrO2	zirconium dioxide	2950	4544	5890	5010	yes	yes
&...	inert species	input	--	input	input	no	no

(1) *Also chemisorbable on steel wall and aerosol particles if Fe and/or Ni are present.*

(2) *Also sorber for chemisorption in aerosol particles.*

(3) *Involved in oxidation reactions with steam and oxygen.*

(4) *Inert as aerosol, not requiring chemical equilibrium or phase change calculation, added by user.*

2.1.3.1 Models for Chemical Reactions in Fusion Reactor Accidents

ECART allows to fit the fusion reactors model for the oxidation reactions of beryllium, graphite and tungsten in air and steam. These reactions involve three features modelled by the code: heat structures, aerosol particles suspended in the carrier gas and aerosol particles deposited on walls.

The reactions of beryllium, graphite and tungsten solid walls of PFCs or dusts with air and/or steam are not explicitly treated by the chemical section of ECART but in a separate ad-hoc module which makes use of surface reactions rates computed by means of semi-empirical correlations, also giving the reaction heats released to or removed from the environment. The basic chemical reactions are [Parozzi, 2000]:

BERYLLIUM-STEAM	$Be + H_2O \rightarrow BeO + H_2 - 370$ kJ/mol
BERYLLIUM-OXYGEN	$Be + \frac{1}{2}O_2 \rightarrow BeO - 610$ kJ/mol
GRAPHITE OXIDATION IN STEAM	$C + H_2O \rightarrow CO + H_2 + 131$ kJ/mol
GRAPHITE OXIDATION IN AIR	$C + O_2 \rightarrow CO_2 - 390$ kJ/mol
TUNGSTEN OXIDATION IN STEAM	$W + 3\ H_2O \rightarrow WO_3 + 3\ H_2$ - 156 kJ/mol of W
TUNGSTEN OXIDATION IN AIR	$W + 3/2\ O_2 \rightarrow WO_3$ - 841 kJ/mol of W

The oxidation reactions are only limited by the availability of steam and oxygen in the carrier gas, while the mass of the reacting element (Be, C or W) in the suspended or deposited aerosol cannot become negative (on a solid wall, the reacted elements Be, C and W and the solid oxide reaction products BeO and WO_3 are not accounted for).

If the amount of steam or oxygen required by all the reactions occurring concurrently, in the current time step, is greater than the available mass, the Δm of each reaction is scaled by the ratio of the available to the required mass of steam or oxygen. In this way, no reaction is favoured but some delay in the reaction completion could result.

Obviously, in a stand-alone aerosol-vapour analysis, no account is taken of the reaction heating and of the mass addition to or subtraction from the carrier gas because the thermal-hydraulic conditions

are fixed by input tables. On the contrary, for the reactions occurring in the suspended or deposited aerosol, the mass increase (or decrease) in a time step or sub-step, of the involved chemical species (e.g., Be and BeO) is allowed for in the mass balance equations and is distributed over the aerosol size bins proportionally to the square of the geometric mean radius of the particles.

If a thermal-hydraulics/aerosol-vapour coupled analysis is performed, the reaction heat (positive for exothermic reaction) is added to the gas atmosphere for reactions occurring in the suspended aerosol and is added to the structure for reactions occurring on the solid surface or in the deposited aerosol.

The masses of the carrier gas components (steam, hydrogen, oxygen, carbon monoxide and dioxide) released or removed by the reactions, as well as the correspondent enthalpies, are accounted for in thermal-hydraulics.

The reactions in the suspended aerosol are assumed to occur at the gas bulk temperature, while the boundary layer temperature (i.e. geometric mean of wall and gas bulk temperatures) is used for the reactions with solid walls and deposited aerosols. This last assumption is questionable and it is under further assessment (at the present, in the code input deck is possible to choose the temperature to be used – bulk or wall).

The reaction area is identified with the wall surface area for the reactions on a solid wall and with the surface area of all the particles multiplied by the mass fraction of the reacted element for the reactions in the airborne aerosol. Also, as far as the reaction area for the deposited aerosol is concerned, the total surface area of the aerosol particles is assumed except when the deposited liquid mass exceeds a given fraction of the total deposited mass, in which case the area of the underlying wall is assumed. However, for a multi-layer deposited aerosol, the basic reaction area should be reduced depending on the depth of the deposited aerosol and on the dispersion (standard deviation) of the aerosol particles distribution, i.e., on the compactness of the aerosol agglomerate.

3. CHARACTERISTICS OF THE ANALYSIS

The present contract between ENEA and DIMNP is the third one inside this EFDA framework for the analysis of a large ex-vessel break sequence in the divertor heat transfer system of the ITER facility, carried out to test the ECART models and get useful indications for future improvements of the code itself.

For the previous ECART analysis on the same sequence [Cambi, 2003], the ITER plant was schematised utilizing 20 control nodes and 29 junctions , also having flow characteristics function of time or pressure. For this previous analysis the focus was on the study of the main thermal-hydraulics path for the transport (by-pass by natural circulation) of Tritium gas and ACP/dust aerosol particles outside the ITER plant, main path formed by the VV (including its engineering safeguards like the drain and the suppression tanks), the divertor cooling loop pipes where the two breaks are located and the Vault. In this new contract, on the contrary, the focus is on the updating of the ITER plant nodalisation according to the new SADL and AAS design data and the comparison of the new results with the Swedish MELCOR results for QA reasons. To allow a better comparison with these MELCOR results, the different assumptions from the SADL data present in the MELCOR analyses have been also maintained in the ECART model (the main discrepancies are highlighted in **bold characters** in the present report).

In particular, to avoid too large uncertainties in the ECART code results, the characterization of the tritium and dust releases and the long term by-pass flow-rate have been carefully assessed in the preparatory phase of the analyses.

3.1 Description of the Accident Scenario

As previously said, the present task is a study of the same **divertor ex-vessel pipe break sequence** taking into account the new features and new parameters of the ITER reactor. The previous developed ECART model [Cambi, 2003] has been updated on the basis of the revised design data reported inside the SADL-4 [Bartels, 2003 a] and AAS [Bartels, 2003 b], performing also a comparison with the Swedish MELCOR data and results (for the thermal-hydraulics main parameters and the radioactive releases to the external environment) for the same sequence reported in [Sheng, 2003].

The main objectives of this particular task, as stated inside the AAS [Bartels, 2003 b], are to show that the overpressure in the Tokamak Cooling Water System (TCWS) Vault and inside the Vacuum Vessel are safely mitigated by the different emergency systems, that the post accident cooling is established and to study the transport of radioactive materials and their release to the external environment. At the same time this analytical study, being also a comparison with the MELCOR analysis, is a step for the quality assurance of the safety analysis of the ITER plant performed in the EFDA framework.

According to the AAS specifications, the initiating event of the LOCA sequence is a double ended pipe break in the divertor cooling loop, which is postulated to occur in the larger diameter pipe of the Primary Heat Transport System (PHTS) cold leg at the inlet of the main circulation pump (see Figure 3.1). The inner diameter of this pipe is 515.0 mm and the break mass flow is discharged into the TCWS vault.

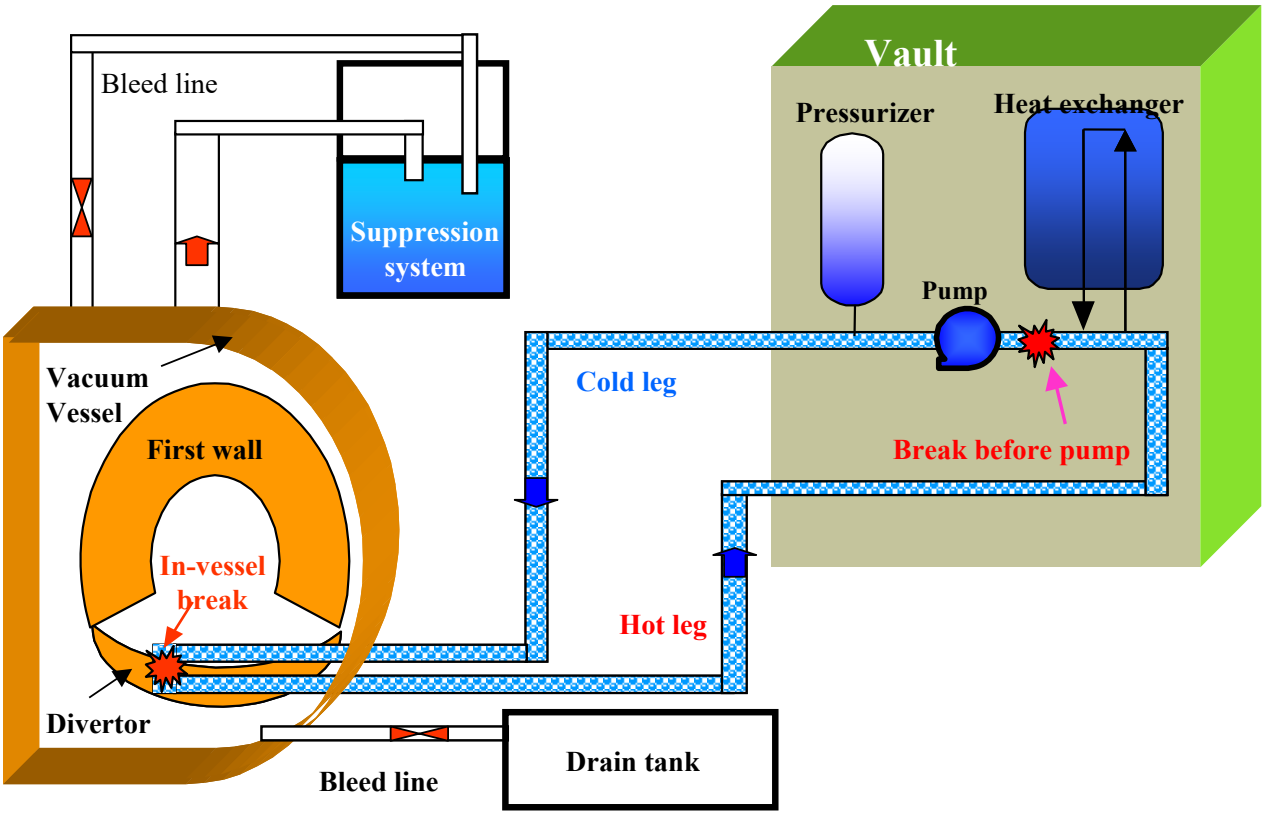

Figure 3.1: Sketch of the accident.

This external break occurs during the plasma burn and, as a consequence of the pipe break itself, the plasma disrupts 3.0 s later. The plasma disruption causes an immediate failure of the DV pipes inside the VV. The internal break size is assumed to be 0.32 m^2, which is equivalent to one toroidal ring, i.e. a break in all the divertor pipes.

The chemical reaction between steam and dust produces 2.8 kg of hydrogen gas inside the VV, as stated in [Sheng, 2003] and imposed in the MELCOR analysis as an input datum. In this ECART task the same quantity of hydrogen gas has been injected inside the VV and the gas mass produced by the different oxidation reactions have not been directly evaluated by the ECART chemical module. The transportation of hydrogen, tritium, dust (**only W in the MELCOR in contrast with the SADL assumptions including also Be and C**) and ACPs has been also taken into account during the ECART analyses.

One hour of "loss of off-site power" is assumed to coincide with the initial pipe break. As a result, the pumps in the DV and VV loops trip at 0.0 s and they are not restarted during the rest of the analysed transient.

For the TCWS vault, the Heating, Ventilation, and Air Conditioning system (HVAC) ducts are closed, with a 30.0 s delay, after the pressurization of the TCWS vault (at 105 kPa) to isolate it. The TCWS vault cooler (nominal cooling power 1 MW) is switched on if the Vault pressure increases above 99.7 kPa.

The DV isolation valves on the PHTS close after 1.0 hour, except one valve, which is assumed to fail to open.

The operation of the bleed line and of the rupture disk to the Vacuum Vessel Pressure Suppression System (VVPSS), reported in Figure 3.2, the rupture disk to the Drain Tank (DT) and the Suppression Tank Venting System (ST-VS) are also taken into account.

The main initial values of the plant status and the set-point that have been utilised in the ECART analyses are summarised in the Table 3.1.

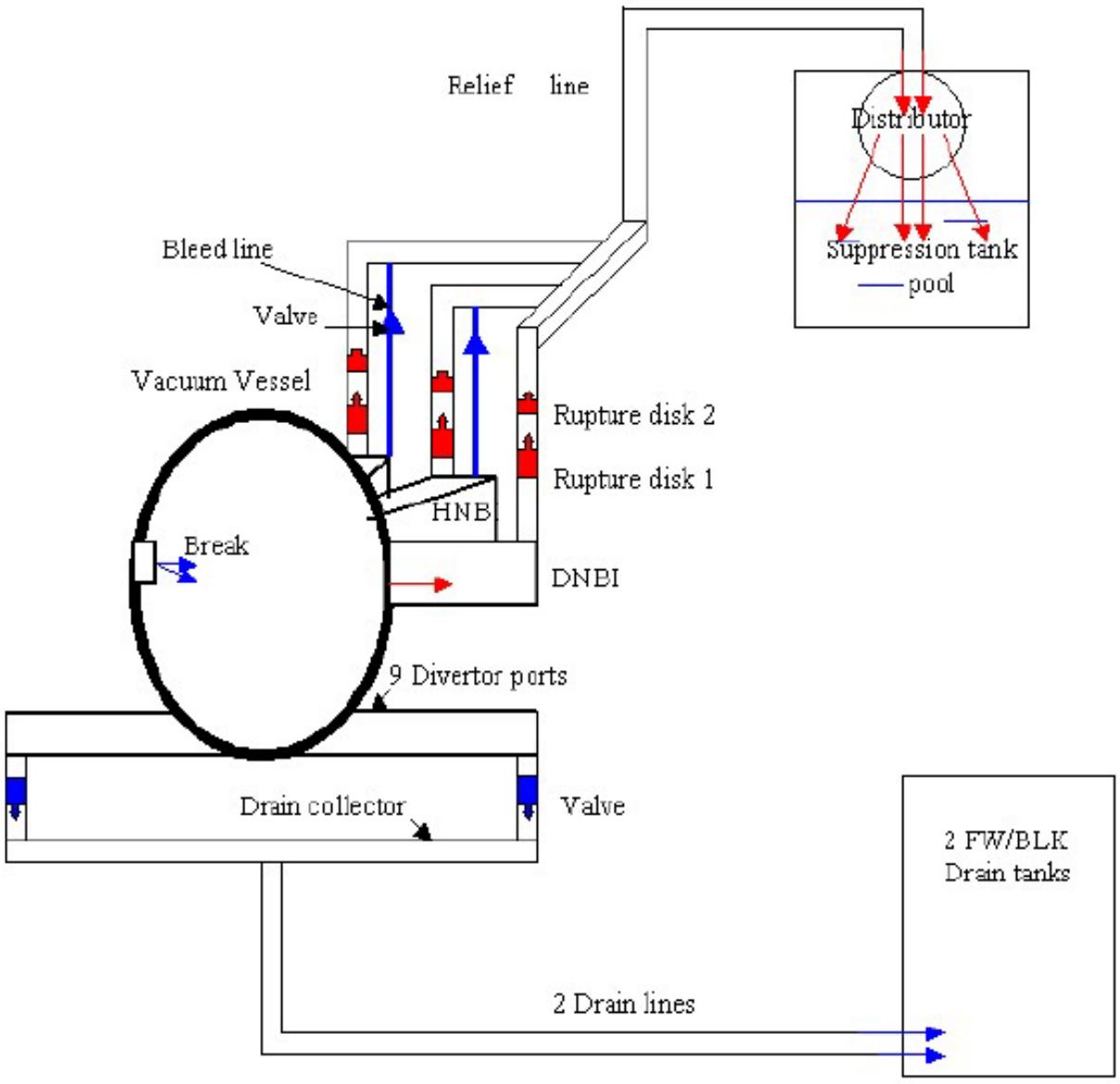

Figure 3.2: VV overpressure mitigation systems.

Parameter	Value
VV	Volume: 1350 m^3 Temperature: 110 °C Pressure: 500 Pa
TCWS vault	Volume: 22970 m^3 Temperature: 23 °C Pressure: 500 Pa Cooling rate: 1 MW Set point for vault cooling: P > 99.7 kPa Time delay for cooling actuation: 30 s
Environment	Volume: infinite Temperature: 23 °C Pressure: 0.1 MPa
Shafts and pipe chases	Volume: 16275 m^3
NBI cell	Volume: 6755 m^3
DV loop	Temperature cold leg: 105 °C Temperature hot leg: 155 °C Pressure: 4.2 MPa
Suppression tank	Volume: 1200 m^3 Temperature: 30 °C Pressure: 4.2kPa (Saturated) Water inventory: 675 m^3 Area bleed lines: 0.05 m^2 Set point for bleed lines opening > 90 kPa Area rupture disk: 0.785 m^2 Set point for rupture disk opening ΔP > 150 kPa
Drain tank	Volume: 409.2 m^3 Temperature: 30 °C Pressure: 4.2kPa (Saturated) Water inventory: 60 m^3 Area rupture disk: 0.0157 m^2 Set point for rupture disk opening ΔP > 110 kPa
ST-VS	Set-point for intervention: ΔP > 90 kPa Time delay for intervention: 180 s Processing rate: 150 m^3-STP/h Filtering efficiency: 99.9%
HVAC	Filter efficiency for particles : 95 % Rating: TCWS vault: 800%/day
S-VDS	Processing rate : 3,000 m^3/hour **Time for S-VDS actuation : 300 s from the beginning of the sequence (in SADL is 105 kPa + 300 s delay)**
TCWS vault leak/in-leak rate	Detritiation efficiency 95% for HTO for first 2 hours Detritiation efficiency 99% for HTO after 2 hours Particle filter efficiency: 99.9% for dust -100%/day x $((\lvert\Delta p\rvert)/300Pa)^{0.5}$ for Δp < -300Pa 100%/day x (1+2(Δp)/300Pa) for –300Pa < Δp < 0 kPa, 100%/day for 0kPa < Δp < 300Pa, 100%/day x $(\Delta p/300Pa)^{0.5}$ for Δp > 300Pa where Δp = P(TCWS vault) – P(Environment)
Set point for TCWS vault/HVAC isolation and for actuating S-VDS	P > 105 kPa
Time delay for TCWS vault /HVAC isolation	30 s

Table 3.1: Initial values and set-points.

3.2 Performed Analyses

As reported in the Studsvik Report on MELCOR analyses [Sheng, 2003], two different parametric case have been performed for this ex-vessel LOCA sequence:

1. **Base Case**
   NO by-pass presence between VV and TCWS Vault trough the cooling loop in the long term phase of the sequence, due to a water plug formation in the DV loop, lasting for 300,000. s.
2. **Removal of Water Captured in DV Loop**
   at about 150 s, an atmosphere flow path opens between the TCWS vault and VV, reduced by the closure of the DV isolation valves (except one) at 3600 s, lasting for 200,000. s.

The first phase of the two thermal-hydraulics transients is identical, as expected, in the ECART analyses, while some large differences are present for the two MELCOR analyses about the total pressure and the wall temperature trends. As general comment, it can be observed as the ECART and MELCOR outputs are more similar considering the parametric case, as will be shown in the following of the report.

3.3 Plant nodalisation

A unique ITER plant general nodalisation, shows in Figure 3.3, has been again set up for ECART in order to permit the assessment of different ITER sequences, according to the Accident Analysis Specifications AAS-4.beta.1 for this project [Bartels, 2003 b]. Only a part of this general nodalisation (reported in Figure 3.9) is employed for this specific LOCA sequence, as better discussed in the following of the report, closing the opportune junctions.

The complete nodalisation appears appropriate as a reference for updating the input database and guarantee coherence among analyses of different scenarios, while simpler nodalisations seem more adequate to analyze specific phenomena or portions of the plant.

All data required to the ITER plant description (geometry, materials, initial conditions, etc.) are taken from the ITER-JWC document “Safety Analysis Data List-4” [Bartels, 2003a]. Other requirements have been also imposed by the necessity, for QA reasons, to compare the ECART results with the results of the same sequence obtained using the MELCOR code [GSSR, 2001] with the limitations above discussed on the predominance of the MELCOR data.

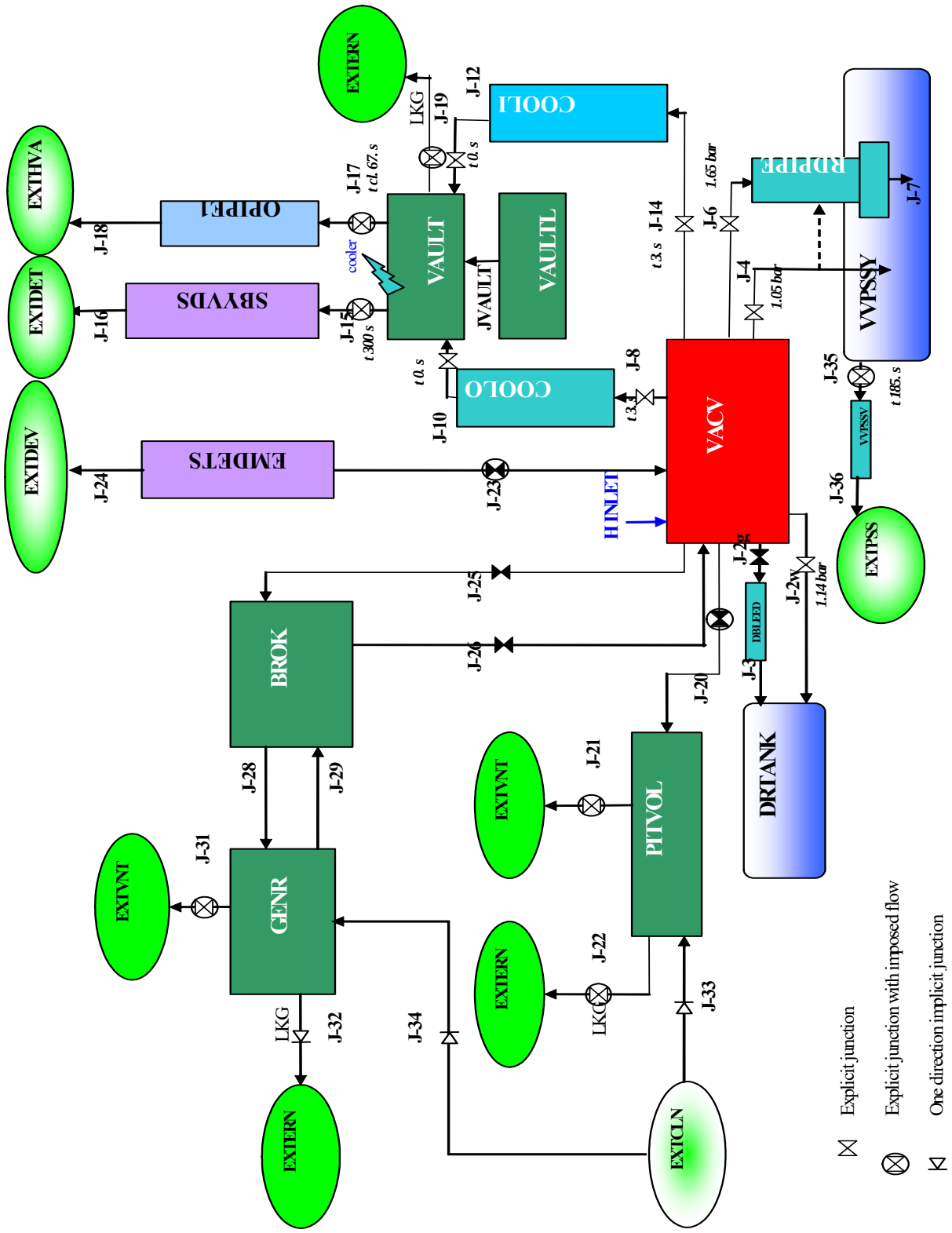

Figure 3.3: Nodalisation of the ITER plant for the ECART code.

This new ECART nodalisation implies 24 control volumes (16 regular volumes and 8 back environments at imposed thermal-hydraulics conditions), 27 heat structures, 9 implicit junctions and 21 explicit junctions, depending on time or pressure, called also in the ECART nomenclature "Spill&Fill". Five non-condensable gases (N_2, O_2, H_2, CO_2, CO) have been accounted for inside the code thermal-hydraulic module plus the tritium gas considered inside the aerosol module. Seven different types of materials and their temperature-dependent thermal properties (carbon steel, stainless steel, concrete, graphite for CFC, W, Be, Cu) have been included in the code input tables, together with two power decay tables for the PFC materials in DV and FW structures, localised on the internal surface of the PFC structures inside the VV. The appropriate boundary conditions (time trends of the external temperatures and of the heat transfer coefficients) have been also imposed for the VV structures, to reproduce the disruption thermal loads and the cooling action of the working HTS.

The broken DV HTS is described in a simplified way, and it is automatically open to the dust and gas/vapour transportation after the end of the coolant blow-down, when the pipe-work system is assumed to be empty and a possible by-pass connection is established between the VV and the TCWS Vault, considering also the DV isolation valves intervention. Two ECART control volumes are employed for the simulation of this HTS circuit: the Cooling Outlet (COOLO) and the Cooling Inlet (COOLI) nodes, also utilised for the calculation of the initial blow-downs into the Vault and into the VV. This nodalisation loop between the VV and the Vault should allows the detection of a possible gas recirculation promoted by natural convection that could cause a long-term tritium and dust transportation from the VV to the TCWS Vault and from the Vault to the external environment. To enhance this recirculation phenomena, in order to have a conservative code prediction of the possible radioactive releases, the outlet from the VV is assumed to be located in the upper portion of this compartment, while the inlet junction is assumed in its lower part. Similarly, the inlet and the outlet inside the TCWS Vault are assumed to be located respectively in the higher and in the lower part of this control volume.

The HTS coolant blow-downs occurring into the Vault (ex-vessel) and into the VV (in-vessel) atmospheres are internally determined by ECART, after a preliminary input tuning of the interested junctions pressure losses on the basis of the MELCOR mass flow-rate results. The predicted ECART mass flow rates are compared with the MELCOR code calculations from Figure 3.4 to

Figure 3.7, showing a reasonable agreement between the two codes. Also if the ECART model does not include coarse models of the DV & the FW/BLK cooling loops (as in MELCOR) but only a very simple model, this coarse nodalisation is however sufficient for:

1. the integrated transport analysis of the radioactive materials;
2. study of the thermal-hydraulic behaviour of the whole system.

The effective employed ECART nodalisation for this sequence of "ex-vessel" break in the DV cooling loop, with a reduction of the control volumes effectively interested by the transient respect to the general nodalisation of the ITER plant, has been obtained simply closing the junctions J-20 (from VV to PITVOL), J-25 and J-26 (from VV to BROK) and J-23 (from VV to EMDETS) and it is reported in Figure 3.9. This reduced ITER model includes the VV, the simplified DV HTS, the PSS (including the suppression tank, the bleed lines, the rupture disks, the ST-VS that starts after the opening of the bleed lines, the DT and its connecting lines/valves) and also a simple two compartments model of the TWCS Vault (lower and upper zone), with its external leakages, the detritiation system (S-VDS) and the venting (HVAC) system.

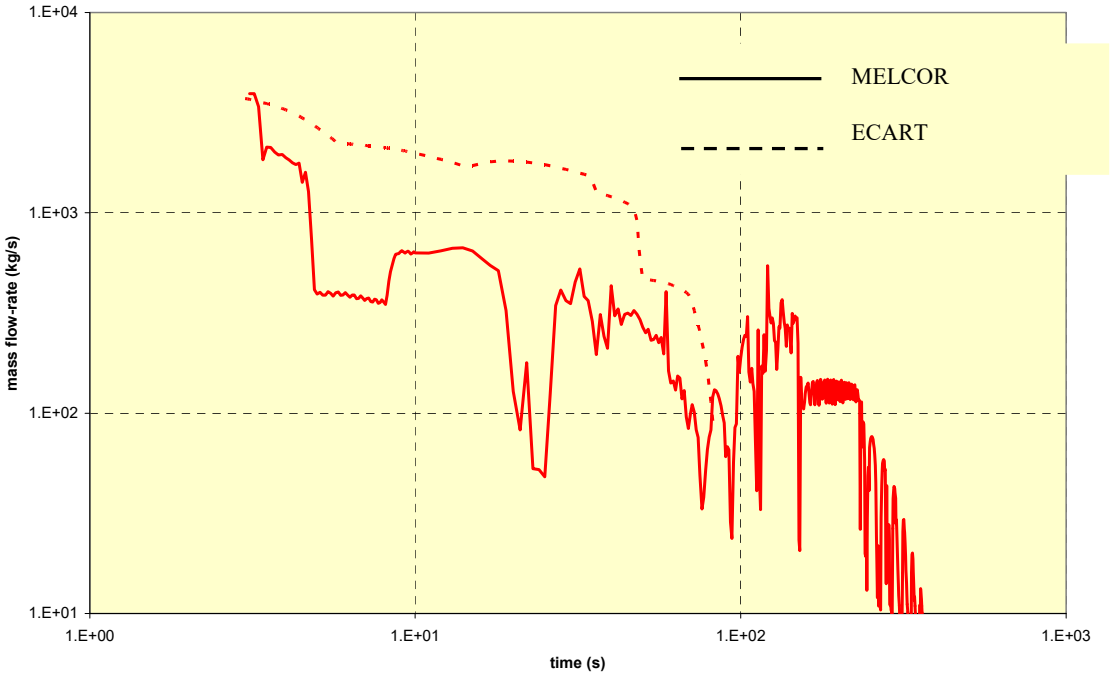

Figure 3.4: Blow-downs predicted by MELCOR and ECART (base case – in vessel).

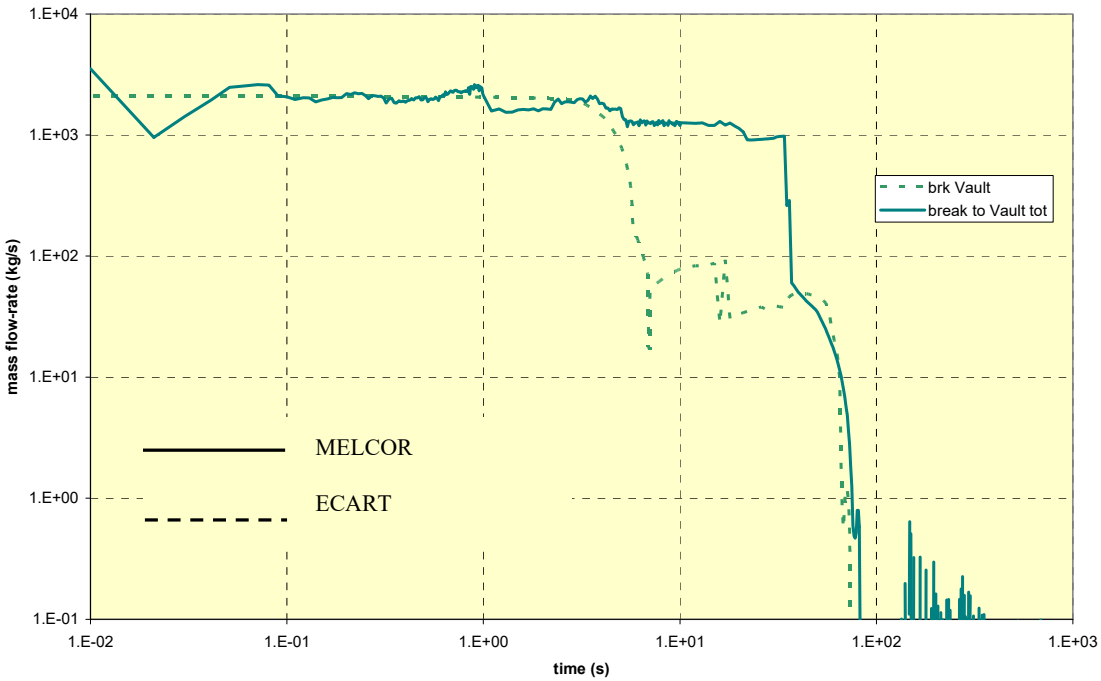

Figure 3.5: Blow-downs predicted by MELCOR and ECART (base case – ex vessel).

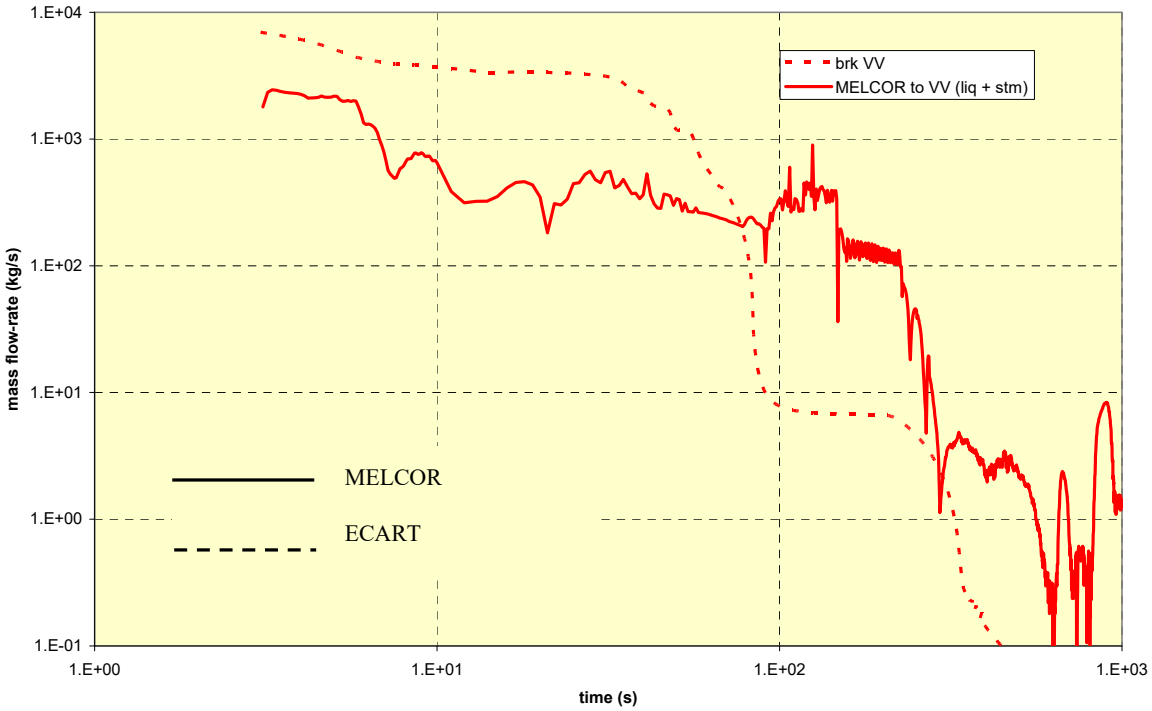

Figure 3.6: Blow-downs predicted by MELCOR and ECART (parametric case – in vessel).

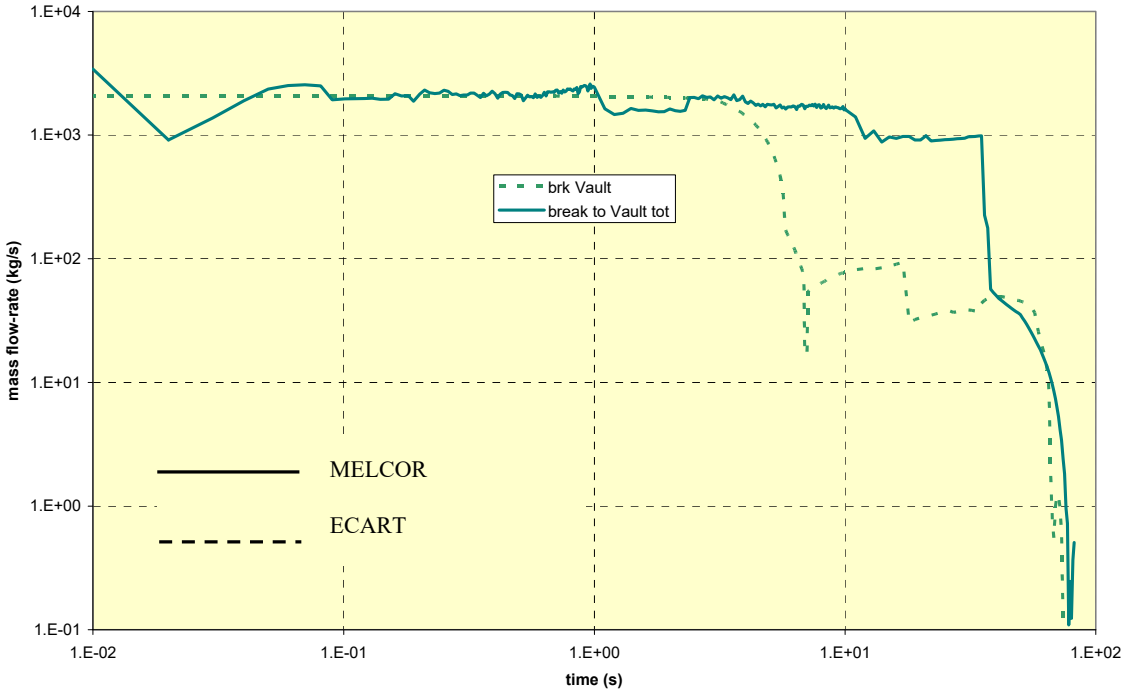

Figure 3.7: Blow-downs predicted by MELCOR and ECART (parametric case – ex vessel).

In the ITER design, the overpressurization of the VV is limited by its PSS, reported in Figure 3.2. This system mainly consists in a big tank partially filled with water (VV PSSY) connected to the VV through:

- a small bleed line (J-4) with an area equal to 0.05 m^2 and equipped with a relief valve, with an opening set-point at 90 kPa;
- a control volume simulating the distributor (RDPIPE), connected with a rupture disk (J-6) of 0.785 m^2 that opens at 150 kPa of differential pressure to the VV and by the submerged vents (J-7) to the tank water pool. For this last junction J-7, the information about the vent submergence has to be specified directly in the input deck.

The presence of this intermediate volume RDPIPE, as for the following DBLEED volume for the DT line, is required by the limitation of the ECART aerosol module in the simulation of parallel junctions connecting the same control volumes. Only a maximum of two parallel junctions is allowed for each couple of control nodes, furthermore mandatory having the inlet and outlet volumes exchanged.

The liquid water drainage from the lower part of VV, when the differential pressure overcomes 110 kPa, is routed through a double line (J-2 for water, located in the bottom of the VV, and DBLEED + J-3 located in the VV atmosphere) into the drain tank (DRTANK).

The VVPSS is equipped with a venting system (ST-VS) which operates in case of a confinement bypass event. Table 3.2, extracted from the SADL, lists the features of this system. This table is the only specific of the ST-VS, present inside the document.

Feature	Value	Unit	Comment
VVPSS-VS efficiency	99.9	%	-
Dust removal efficiency	99.9	%	-
Processing rate	150	m3-STP/hour	Target is to maintain flow velocity of >1 m/s at 0.02 m2 bypass break to avoid any diffusion of radioactivity through break.
Trigger for VVPSS-VS: Pressure in the VV	90	kPa	Same as set point for bleed line
Time for VVPSS-VS start up	3 minutes (tbd)	minutes	-

Table 3.2: Features of the VVPSS venting system (VVPSS-VS).

It has to be immediately highlighted as the ST-VS characterisation needs a better specification respect to the few words present inside the SADL. As a matter of fact, this component is critical for the long term thermal-hydraulic behaviour of the whole system as showed in the parametric analysis on “Removal of Water Captured in DV Loop” reported in Figure 3.8. Changing the characterisation of the pressure losses along the by-pass circuit between the VV and the TCWS Vault and the capacity (in terms of mass flow rate) of the ST-VS system a bifurcation is possible for the by-pass VV-Vault occurrence because the ST-VS mass flow-rate is very near to the air mass flow-rate entering from the Vault into the VV. A different pressure trend, with no reduction (full lines in the figure) of the pressure level of the whole system at the DV isolation valve actuation is possible vs. the reduction presents in the MELCOR & ECART analyses (dotted lines) where a questionable constant volumetric flow simulation, as in the SADL data, for the ST-VS is adopted, also at very low pressure levels inside the ST. The necessity of a realistic characteristic curve for this ST-VS system is clear, to obtain a more reliable simulation of the long-term system transient.

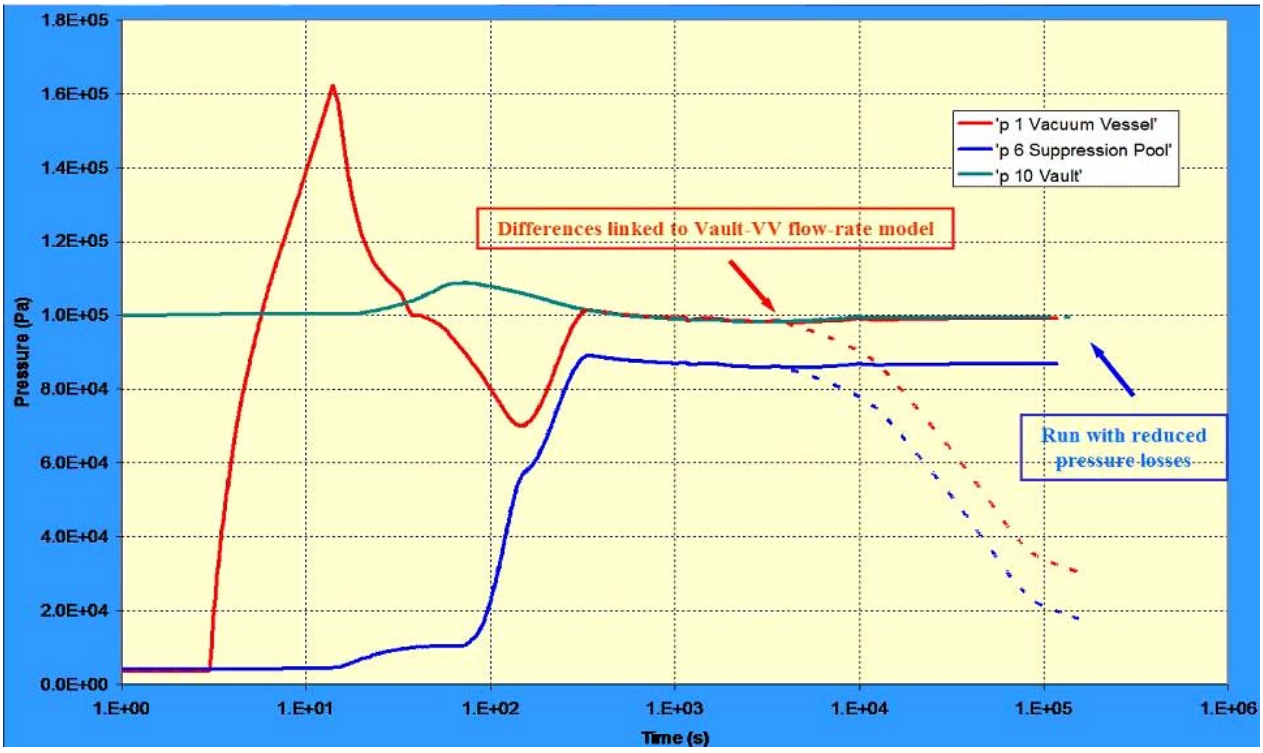

Figure 3.8: Influence of the ST-VS characterisation on the system behaviour (parametric case).

In the ECART nodalisation, all the possible flow-paths for the radioactive releases towards the external environment are separately evaluated. In general, all the ITER plant large parts involved in accident analyses are assumed to possibly discharge/intake the polluted/clear stream into/from an external environment, distinguishing both the pathway and the origin (and, of course, the leakages/intake law). However in the presented analyses no leakage is simulated from the VV (**assumption in contrast with the SADL, where a leakage towards the PITVOL is required**), the DT, the PSS and the ST-VS. This releases simulation has been obtained by assigning seven different "back-environment" volumes in the nodalisation:

1. Discharge by leakages from the Pit Volume (into EXTERP);
2. Discharge by leakages from the General Room and Vault (into EXTERN);
3. Discharge from venting by Pit Volume and General Room (into EXTVNT);
4. Discharge from VV through the EDS (into EXTDEV);
5. Discharge from PSS through the PSS-VS (into EXTPSS);
6. Discharge from the Upper Vault Trough HVAC (into EXTHVA);
7. Discharge from the Upper Vault through the Stand-by Vent Detritiation System S-VDS (into EXTDET).

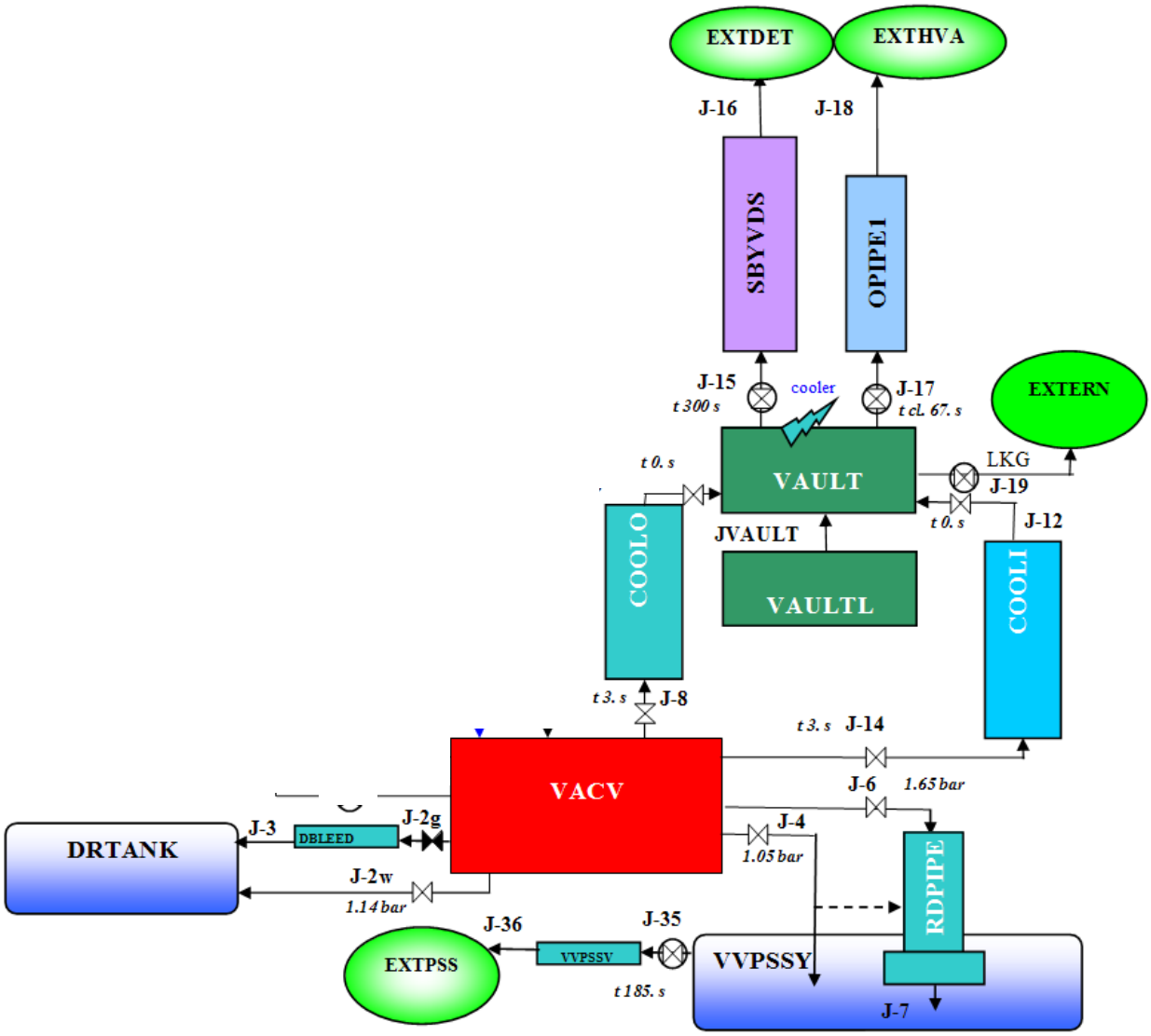

Figure 3.9: Nodalisation of the ITER LOCA sequence for the ECART code.

A further back-environment, simulating the external clean atmosphere (EXTCLN), has been added in order to take into account the air extraction due to the forced ventilation inside the Pit Volume (J-33) and the Generic Room (J-34).

The controlled discharge (H-VAC) from the TCWS Vault atmosphere to the external (EXTHVA volume) occurs through a stack (J-17) and the gas stream flows through a long pipe (OPIPE1). Under accident conditions, when the gas pressure and radioactivity inside the Vault exceed prefixed set points, the gas stream is routed (J-15) through the Stand-by Vent Detritiation System (S-VDS)

into the EXTDET volume. The uncontrolled leakages from this volume to the EXTERN back environment are input specified as a function of the differential pressure with the law from SADL, reported in Figure 3.10.

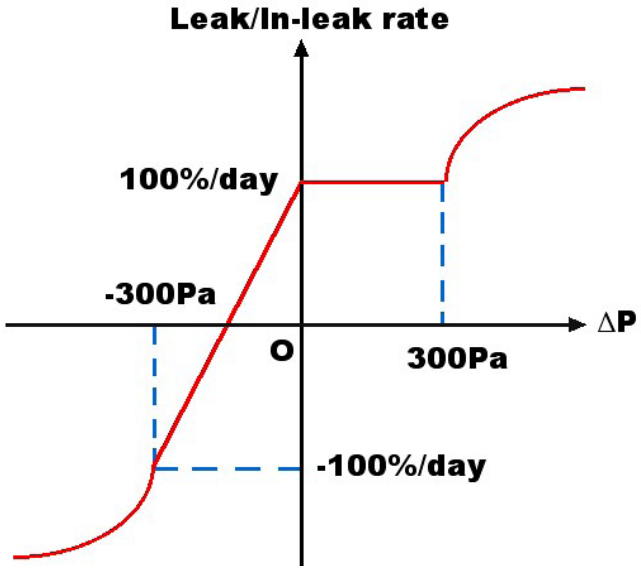

Figure 3.10: Leakages law as a function of the differential pressure.

As previously said, the VV leakage due to overpressurization is not considered in the MELCOR analyses and consequently also in ECART, notwithstanding the SADL specifications. On the contrary, in the complete nodalisation this leakage (J-20) is conveyed to a Pit Volume (PITVOL), representing the room hosting the VV and the PSS. The law of the mass flow-rate as a function of VV pressure for this leakage, as for the other leakages simulated in the nodalisation, has to be input specified, for the lack inside the ECART code, of a specific model for this kind of containment leakages (percentage at day of the total free volume at the design pressure).

For the same reason, **also the Emergency Detritiation System (EMDETS) connected with the VV is not considered in the presented analyses**. In the complete nodalisation it connects the VV with the external environment (EXTDEV) through junctions J-23 and J-24, only in the case of air entering into the VV.

3.4 Tritium and Dust Initial Inventories

The inventory and characteristics of tritium and others activated materials involved in the accident are taken from the MELCOR input [Sheng, 2003] **being the utilised input data sometime strongly different from the SADL 4.beta.1 ones**.

- **Tritium** 0.005 g-T/m3 as concentration in the DV HTS coolant (no information about mobilisation in air) plus 450 g released in VV atmosphere as HTO (63% mobilized at disruption, 37% during 6 h); **on the contrary, in SADL 1000 g of tritium have to be released into the VV atmosphere (50% mobilized at disruption, 50% mobilised in 6 h) with a full mobilisation (as a gas? – unclear point in SADL);**
- **DUST** 5 kg of W dust generated from the disruption plus 350 kg of W mobilized from the in-vessel components. **Only W is taken into account in MELCOR analyses but in SADL also a Be dust (100+5 kg) and a C dust (200+5 kg) are in the dust inventory inside the VV**. According to SADL, all the mass of these dusts are assumed to be suspended in VV atmosphere because of the strong initial resuspension forces caused by the inlet of the coolant blow-down;
- **ACP** 10 kg/loop, contained inside the water of the DV HTS with a mobilization factor equal to 1.3% of the Activated Corrosion Products (ACP) content in the break mass flow. The mobilised ACP are assumed to be instantaneously mixed with the other dusts in the VV and Vault atmosphere.

Investigations are under way [Paci, 2004 c] to estimate the mobilisation (i.e. the re-suspension fraction) of the VV dust inventory. For the present analysis, it has been considered as homogeneously suspended (100% of the total) inside the VV and Vault atmospheres at the beginning of the coolant release, as conservative assumptions.

About the physical status and the initial granulometry of the three different species, sometimes unclear also in the SADL, the assumptions reported in the following Table 3.3 have been imposed for ECART.

Species	type	GSD	AMMD	comments
W Dust **No C or Be**	5 kg	**?**	**SADL: 0.01 µm (AMMD?)** MELCOR: 0.12 µm	as suspended particles
	350 kg **1000 kg in SADL**	2.0	2.11 µm	
ACP	10 kg/loop, mobilization 1.3%	**?**	2.0 µm	as suspended particles
Tritium	Inside VV	**?**	MELCOR: HTO particles 0.12 µm	*possible prediction of a too high retention for thermo-phoresis or diffusional deposition*
	in HTS water		MELCOR: liquid, with no mobilisation?	**gas for SADL? Stated a mobilisation factor 100%**

For the unknown GSD a value equal to 1.1 has been assumed in the ECART analyses

Table 3.3: Physical status and the initial granulometry of the different species.

All the dust or ACP particles are assumed to have a standard "dry" spherical shape (both the dynamic shape factors equal to 1.0). This assumption is questionable for the strong presence of liquid water inside the VV and Vault, that increase these shape factors leading to an increase of the particles agglomeration [Parozzi, 1997b]. However, this "dry" assumption is conservative because larger particles have a higher gravitational deposition velocity and so this retention process, in this way, is minimised.

4. ECART RESULTS AND COMPARISON WITH THE MELCOR DATA

The analysis of the ECART results again confirms the capability of the ITER design to avoid critical situations about the radiological releases to the external environment also for this particular sequence, that is one of the most severe for the environmental impact.

In the following the ECART results, about both thermal-hydraulics and radioactive releases, will be analyzed and compared with the MELCOR results from Studsvik Neclear [Sheng, 2003].

4.1 Main Thermal-hydraulics Results

First of all it has to be highlighted as there is a quite good general agreement between the ECART and MELCOR results for the overall thermal-hydraulics behaviour of the ITER Plant for this particular severe sequence. The comparison of the calculated sequence timing for the two codes is reported in the following Table 4.1 - for the base case - until the DV isolation valves activation at 3600 s.

Event	MELCOR Time (s)	ECART Time (s)
Ex-vessel pipe break and loss of off-site power	0.0	0.0
Plasma disruption	3.0	3.0
In-vessel pipe break	3.0	3.0
Opening of bleed line to ST	4.8	6.0
Opening of rupture disc to DT	5.4	6.8
Opening of rupture disc to ST	10.4	14.0
Closing of HVAC ducts	66.4	67.0
Start of ST-VS	184.	185.
Start of S-VDS (time imposed)	300.	300.
Closing of DV isolation valves (time imposed)	3600.	3600.

Table 4.1: Comparison of the sequence timing for the base case.

However, notwithstanding the good general agreement, the pressurization trends inside the VV, DT and PSS for the base case (Figure 4.1) show a temporal shift caused by the two different timings of

the ST rupture disk openings (10.4 s vs. 14.0 in ECART). This effect is due to the different approach in the modelling of the HTS circuit, more detailed and realistic for the MELCOR code. As a consequence, a slower HTS depressurization rate is predicted by ECART, consequently leading to a slow pressurization rate of the VV and of the whole system. On the contrary, for the parametric case (Figure 4.2), the agreement between the two codes for the VV pressurisation trend is quite good. It is unclear the reason of the differences in the MELCOR results between the base and the parametric cases (also for the VV blow-down flow-rates, as reported in Figure 4.3), because the initial part of the sequence should be not influenced (as in ECART) by the water plug formation inside the HTS broken loop.

For the same reason, the set points for the PSS rupture disk opening are reached at about 10 s from the accident start for MELCOR base case and at about 15 s for the MELCOR parametric case and in the two ECART runs.

In ECART, the set point for TCWS vault isolation is reached after about 40 s from the accident start, therefore considering the required delay, a closure time of about 340 s was inferred by SADL data. On the contrary, considering the MELCOR nodalisation of the sequence, the **Vault was isolated from the environment at 300 s sharp**, with a time trip. This shorter assumption is surely not conservative about the consequent external releases.

Considering these pressure results, it is possible to conclude that, almost for the base case, all the ECART events are delayed compared to those of MELCOR while a better agreement is present for the parametric run. For this last case, the critical point is the estimation, after the closure of the DV isolation valves (except one), of the correct balance between the air mass flowing into the VV trough the in-vessel break and the ST-VS suction capacity (Figure 4.4). In both the calculations, on the basis of the high ST-VS suction capacity specified in SADL, as above discussed, a strong depressurisation of the VV is predicted after 3600. s with the consequent impossibility of a long term release of the radioactive materials still present inside the VV. On the contrary, in the old analysis [Cambi, 2003], the VV depressurisation was not predicted (the ST-VS was not present) and a possible radiological by-pass was calculated. But also in this new case the uncertainties about this particular point are quite high, considering also the small difference in the ST-VS capacity and the air flow entering into the VV (Figure 4.4).

Also regards the atmosphere temperatures and the surface temperatures of the PFC heat structures, the agreement between the two code is worst in the base case (Figure 4.5) respect to the parametric

run (Figure 4.6). Again is difficult to understand the reasons of the strong differences present in the two MELCOR runs especially for the VV atmosphere temperature that in ECART is always strongly linked to the VV wall one. The same temporal shift in the ST atmosphere temperature trend is predicted by ECART, as for the pressurization rate previously discussed.

Concluding, this comparison of the two different codes gives a quite good qualitative and quantitative agreement in the main thermal-hydraulic results; i.e. the mass flow-rates from the different breaks are comparable, the pressure peak in VV, DT and VVPSS and the long-term equilibrium pressure of the whole system are very similar.

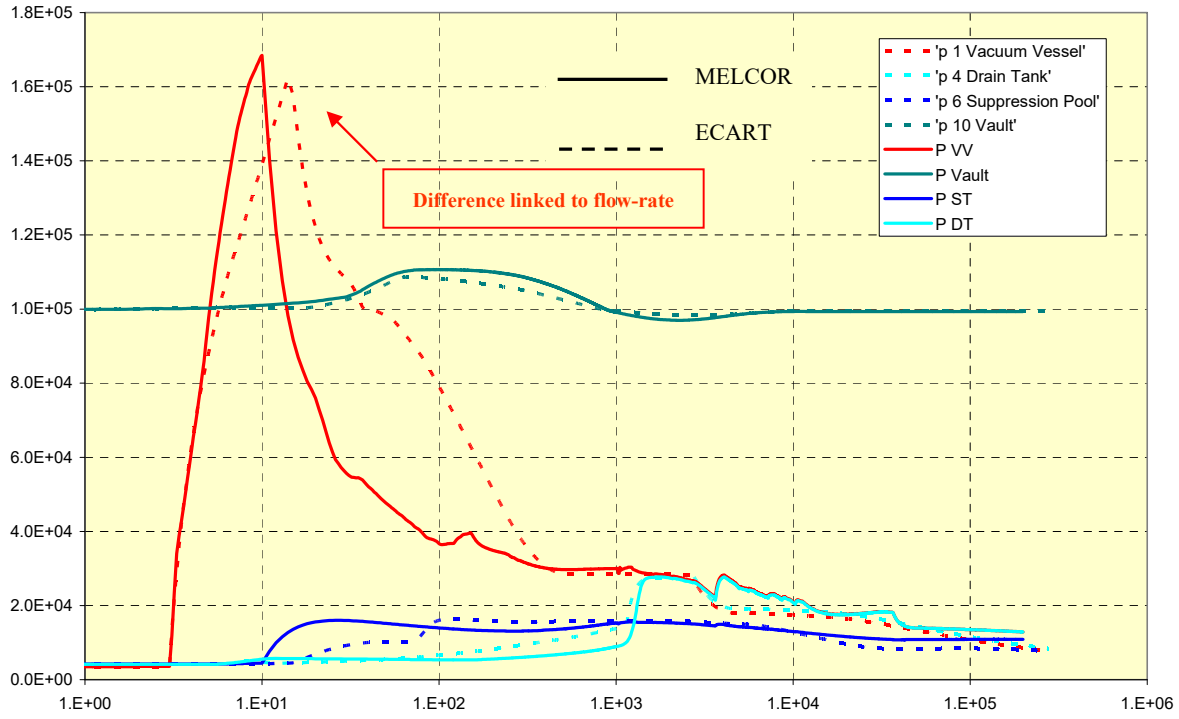

Figure 4.1: Base case - pressure trends inside VV, ST, DT and TCWS Vault.

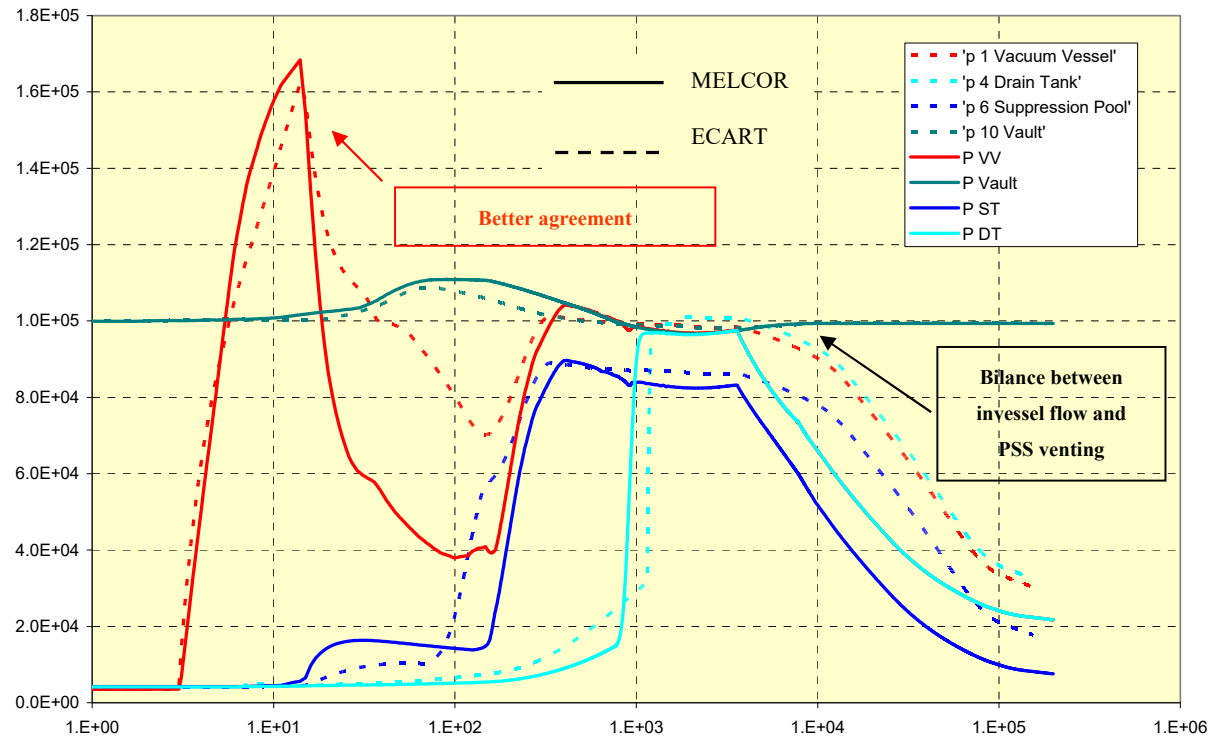

Figure 4.2: Parametric case - pressure trends inside VV, ST, DT and TCWS Vault.

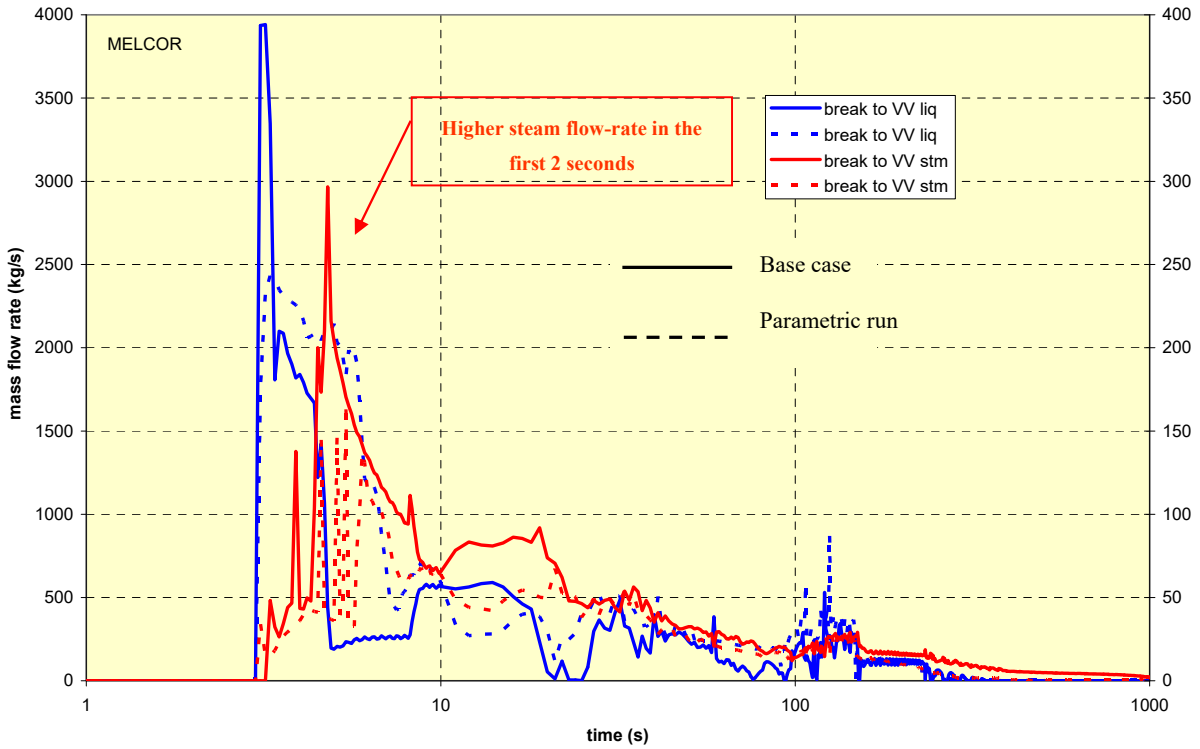

Figure 4.3: Base case – MELCOR flow-rates into the VV.

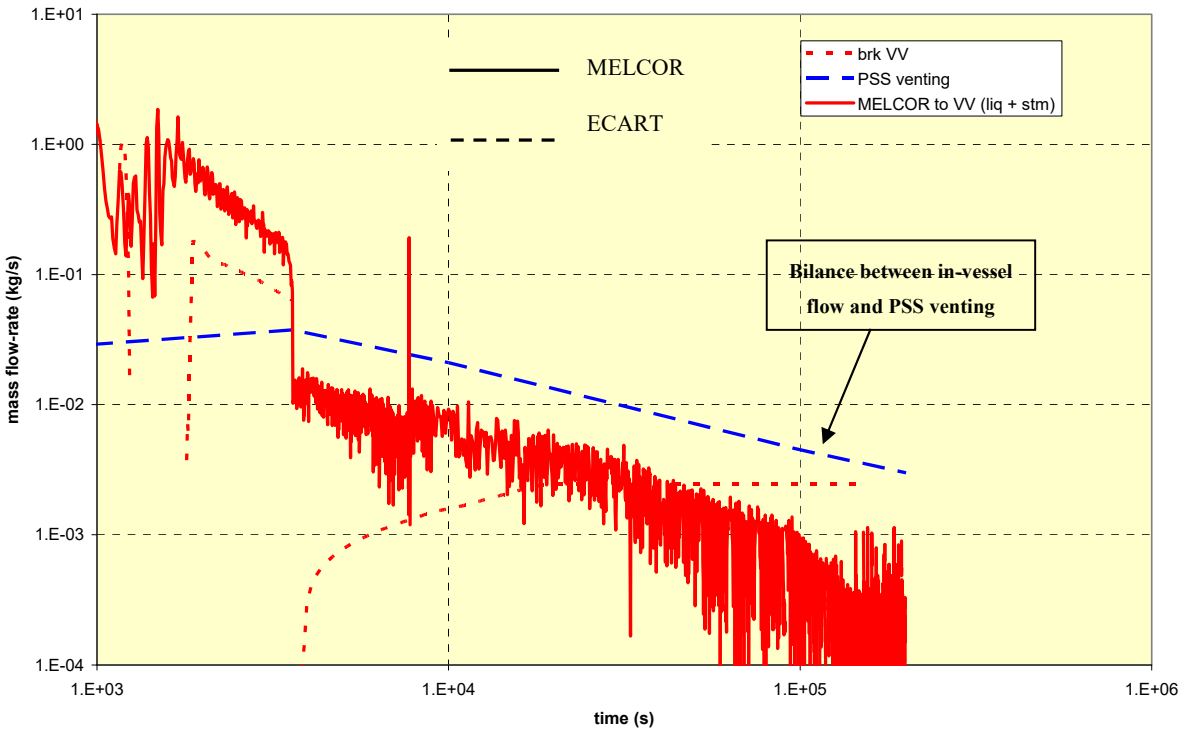

Figure 4.4: Parametric case – Long term flow-rates into the VV.

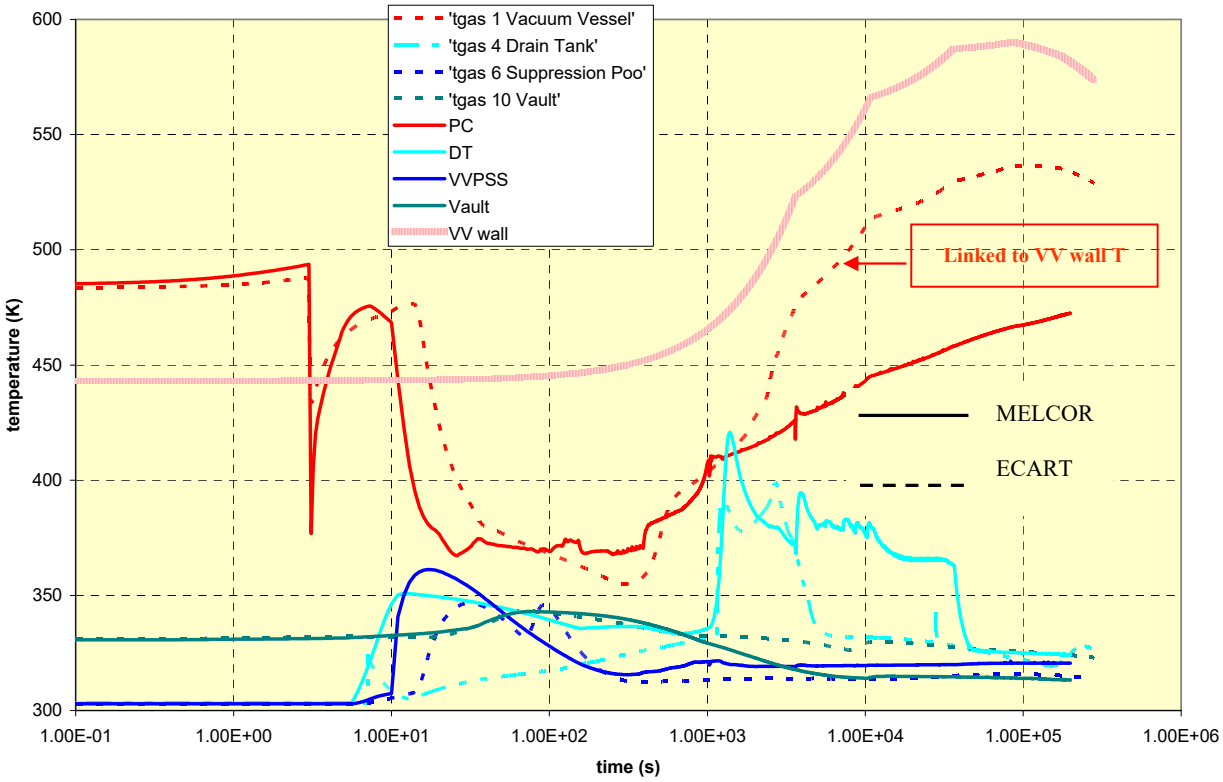

Figure 4.5: Base case – Temperature trends.

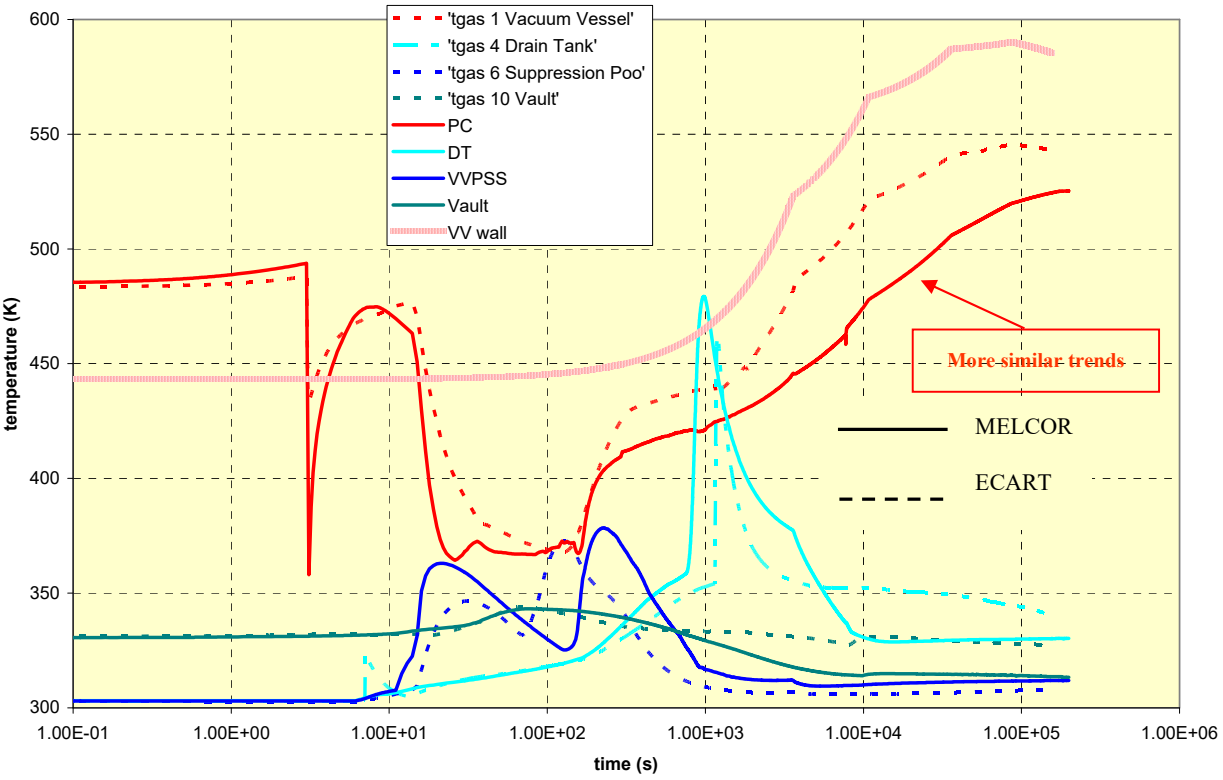

Figure 4.6: Parametric case – Temperature trends.

4.2 Dust, ACP and Tritium Transport Results

The results obtained with the ECART aerosol models, already tested and validated in the framework of several fission reactor studies [Wright, 1994; Jones, 2001], are promising also in the fusion safety field [Paci, 2004 b] but, because the inventory of radioactive materials released to the external environment is low, to confirm the correctness of the present "code vs. code" assessment, future experimental analyses could be addressed to study the particles behaviour in specific circuit parts, as the dust resuspension inside the VV, or components as the ST-VS influencing the release itself.

Summarising the global results about the releases of the three radioactive species considered in the present analyses to the outside environment (via four flow-paths, three for the TCWS Vault - leakages, S-VDS and HVAC - plus the ST-VS), ECART - like MELCOR - predicts very negligible and comparables amounts for T, W and ACP (reported unfiltered, for a better comparison, in Figure 4.7 and Figure 4.8 respectively for the base and the parametric case). These results also confirm the independent MELCOR analysis reported in [Topilski, 2004]. In the following of the report, these external releases of the different radioactive materials will be in deep analysed and compared, after some general comments on the different behaviours of the 3 materials.

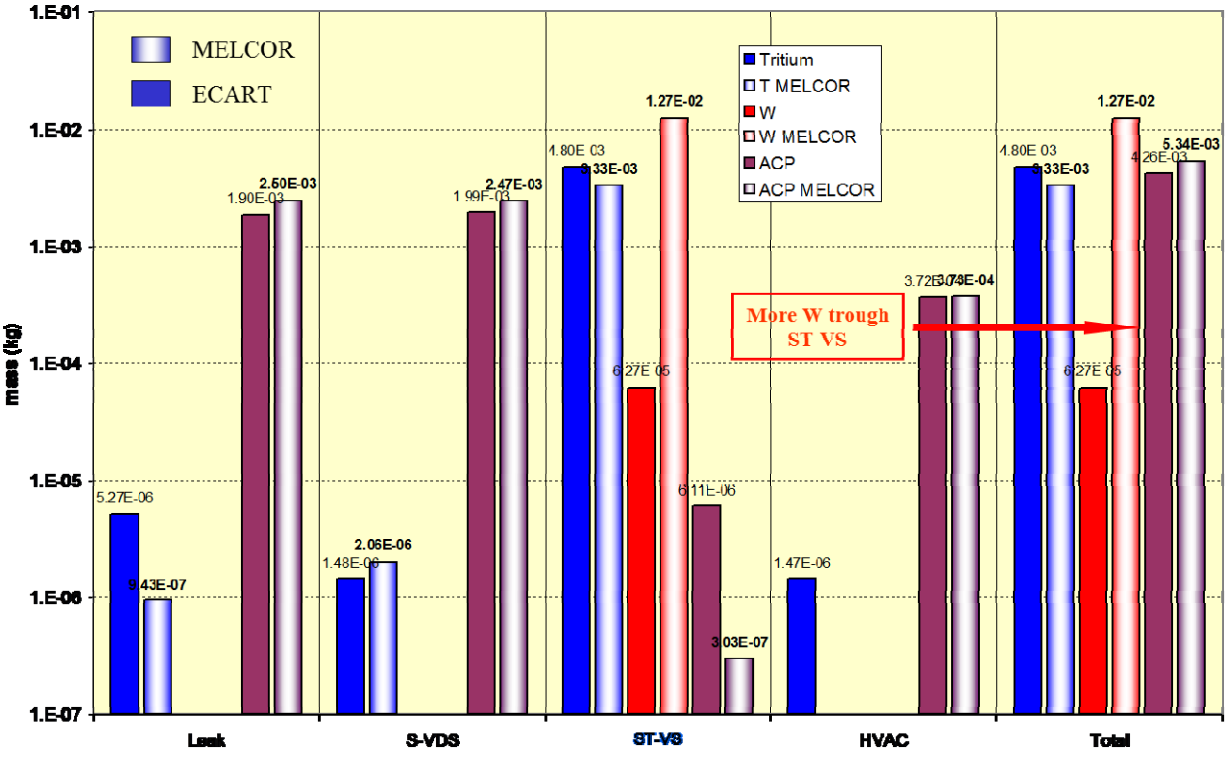

Figure 4.7: Base case - Unfiltered Releases of radioactive species.

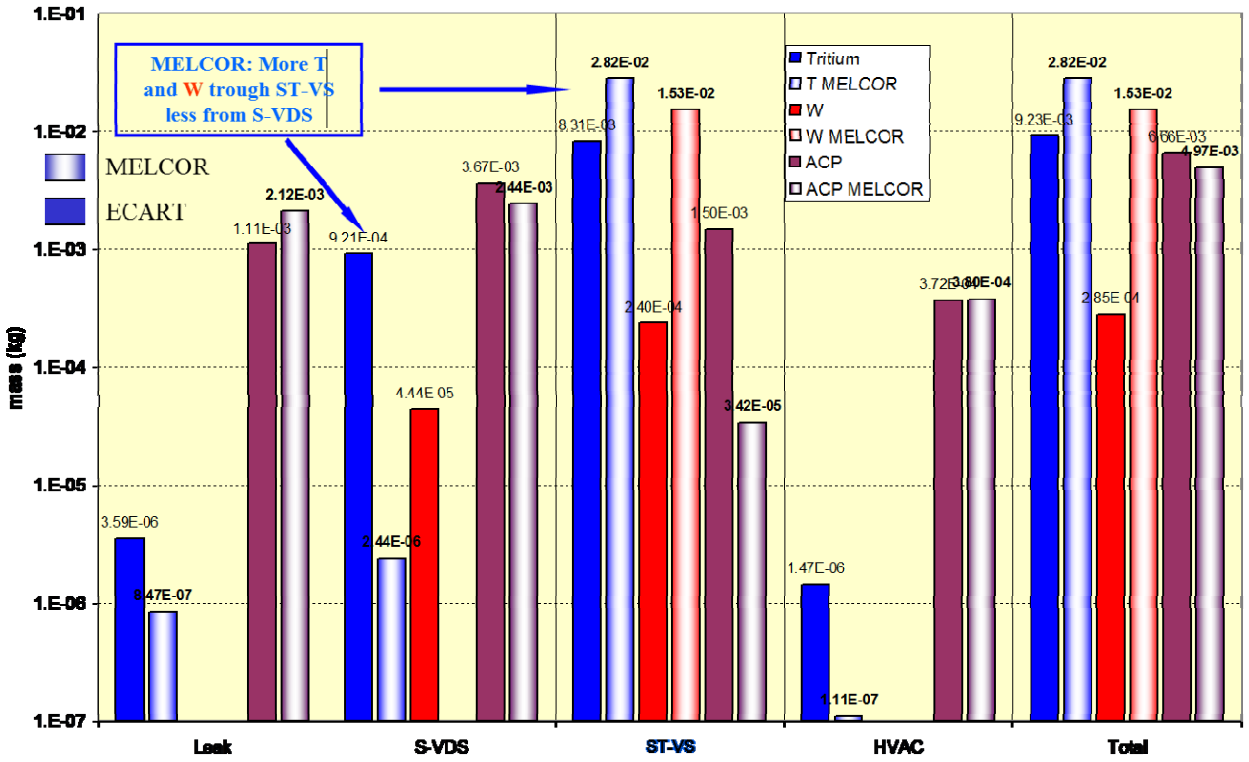

Figure 4.8: Parametric case - Unfiltered Releases of radioactive species.

The Tritium transport is considered in both the codes to occur as HTO particles (not as a gas or a vapour) having a small AMMD of 0.12 μm, practically with weak depletion mechanisms also for the scrubbing in the suppression pool[2]. Its releases from the plant is then mainly due to the ST-VS, where a significant fraction of the Tritium inventory is pushed. Obviously, the delayed opening of the VV rupture disks, accounted by ECART for the base case, contributes to increase the Tritium transport towards the TCWS Vault and, consequently, into the external environment; on the contrary, in the parametric run, more HTO is transported through the ST-VS. Obviously, if the HTO would be considered as a gas, larger releases would be predicted.

A better agreement between the two codes predictions is highlighted considering the ACP releases, having a physical status and a granulometry clearly defined by the analysis specifications. It has to

[2] A more complex model for the HTO transport in liquid or vapour form should be required for the evaluation of its retention inside a pool, considering its chemical equilibrium with the steam and liquid water, always present inside a control node. This particular model, at the moment, is not implemented neither in ECART nor in MELCOR, leading to questionable results for HTO releases.

be remembered as the major part of the ACP particles is released from the HTS coolant directly into the VV or the TCWS Vault atmospheres in the initial phase of the accident, bypassing all the retention phenomena along the DV HTS piping.

About the W dust, ECART predicts a higher scrubbing effect than MELCOR inside the ST pool, with consequent lower ST-VS releases. Being unknown the pool scrubbing model implemented in MELCOR a comparison is practically impossible. About the S-VDS dust release, predicted by ECART for the parametric case only (no W release for both the codes for the base case), it is strongly influenced by the flow-rate values of the natural circulation flow between the VV and the TCWS Vault, being this low flow the carrier for driving the W dusts from the VV atmosphere into the Vault, where they will be released into the external atmosphere mainly by the Vault leakages and by the S-VDS.

In the following, from Figure 4.9 to Figure 4.14, the total mass[3] of the three radioactive species (Tritium, W and ACP) present inside three different control volumes (VV, TCWS Vault and ST) will be compared for the two codes.

Inside the VV (which conditions are respectively reported in Figure 4.9 and Figure 4.10 for the base case and the parametric case), the following phenomena are quite evident:

a) the short term influence of the difference for the RD opening times for the W and HTO masses. This influence is further confirmed by the good agreement for the Tritium mass data in the parametric case, where the RD opening time, as previously discussed, is equal between the two codes;

b) the absence, in the MELCOR results, of the HTO specie in the long term phase of the sequence, also as deposited mass; it is quite difficult to explain this fact, for lack of information, and this result is also responsible for the different HTO behaviour in the TCWS Vault;

c) the strong errors in the initial masses of W and HTO in the parametric case for MELCOR, repeated in ECART to allow a comparison of the sequence;

d) the very low quantity of ACP mass present inside the VV for all the analyses.

[3] No MELCOR plot data are available for the “suspended” mass of the specific material; available are the “suspended + pool deposited” mass or the “deposited on structures” mass.

For the masses inside the TCWS Vault (respectively reported in Figure 4.11 and Figure 4.12 for the base case and the parametric case), the codes agreement is quite good considering the suspended masses of Tritium and ACP in the base case while a stronger “by-pass effect” is predicted by ECART for HTO and W masses in the long term phase of the parametric sequence. It’s unclear why the MELCOR code does not predict this “by-pass effect”, considering the pressure difference between the two volumes reported in Figure 4.15. Possible explanations are that no Tritium mass is suspended inside the VV for transportation to the TWCS Vault in MELCOR or, again, problems linked to the Tritium characterization.

Inside the ST volume (masses respectively reported in Figure 4.13 and Figure 4.14 for the base case and the parametric case), its quite evident:

a) the good agreement about the ACP mass and also the concordance between the two codes results for the W and the HTO masses, excluding the long term behaviours;

b) the strange long tem behaviours predicted by MELCOR for the W and the HTO masses, with non linear trends in the base case, in comparison to the linear ECART ones;

c) the linear long trend behaviour for the W mass, in the parametric case, also for the MELCOR code;

d) the unclear sharp increase in the T mass inside the ST predicted by MELCOR in the parametric case.

The consequent releases to the external environment will be discussed in the following paragraph on the basis of the just presented phenomenology inside the three main control nodes.

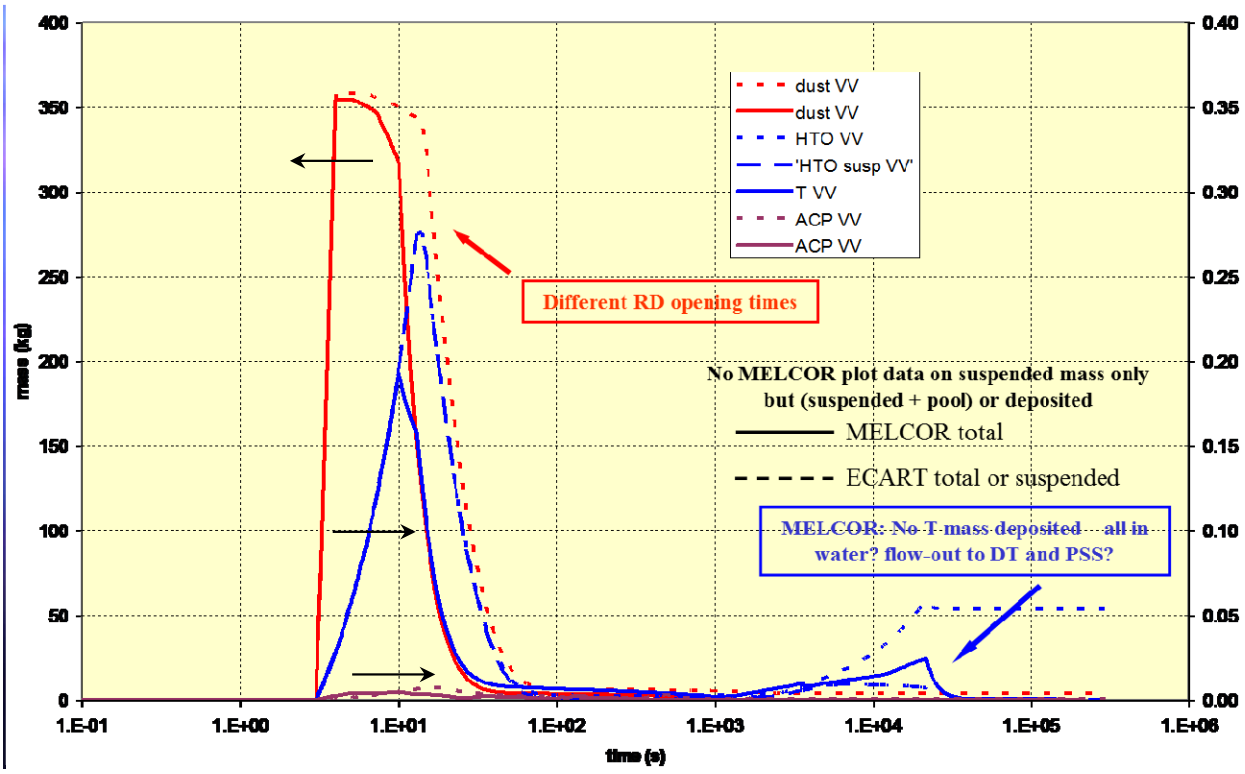

Figure 4.9: Base case – HTO, W and ACP inside the VV.

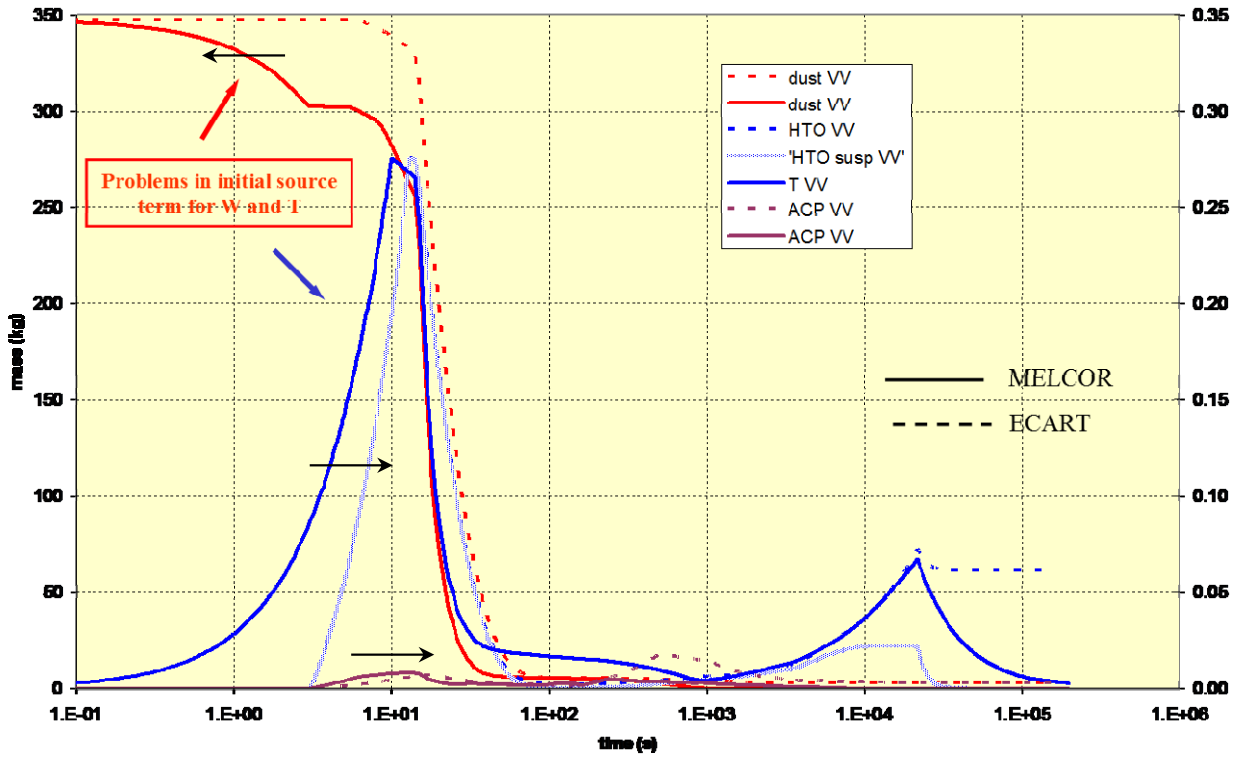

Figure 4.10: Parametric case – HTO, W and ACP inside the VV.

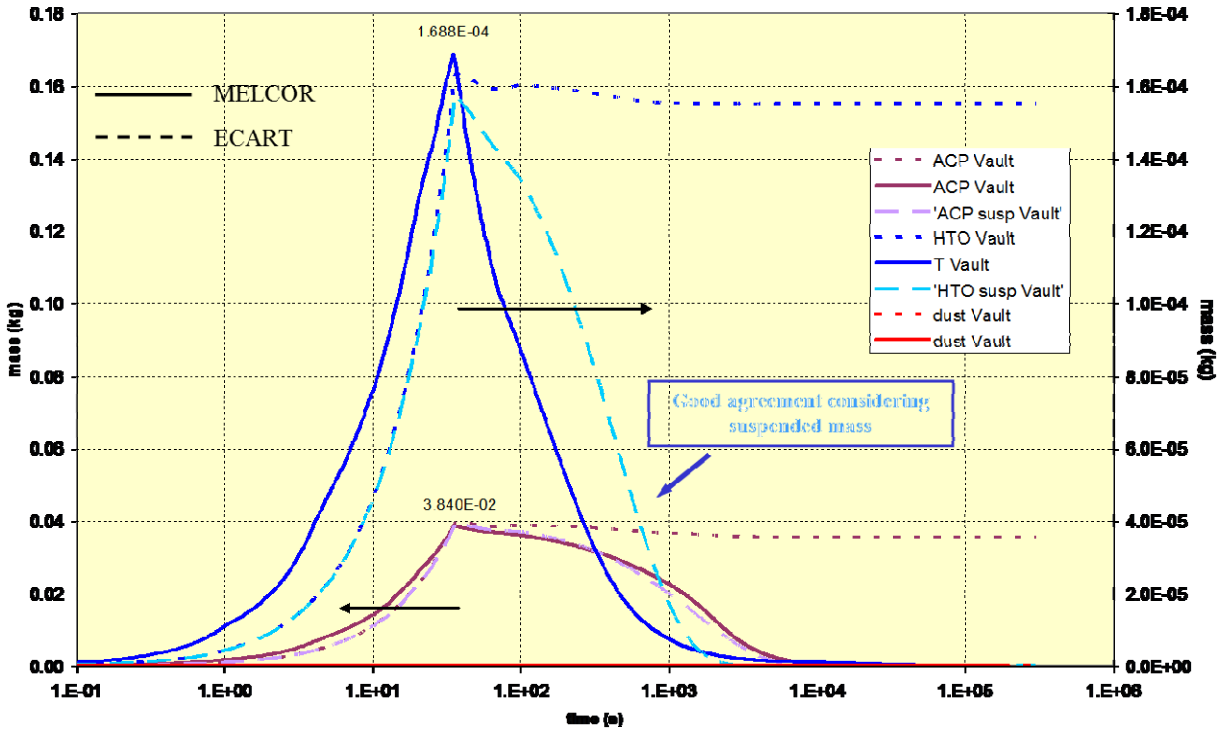

Figure 4.11: Base case – HTO, W and ACP inside the Vault.

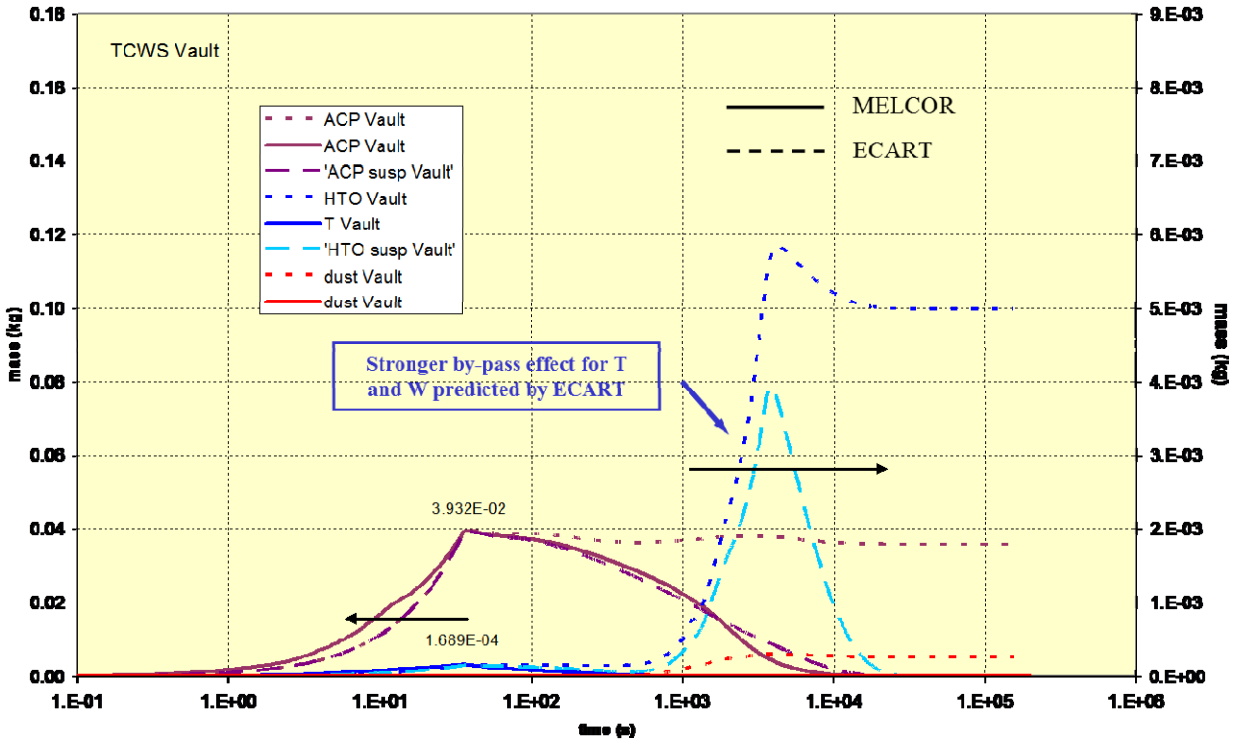

Figure 4.12: Parametric case – HTO, W and ACP inside the Vault.

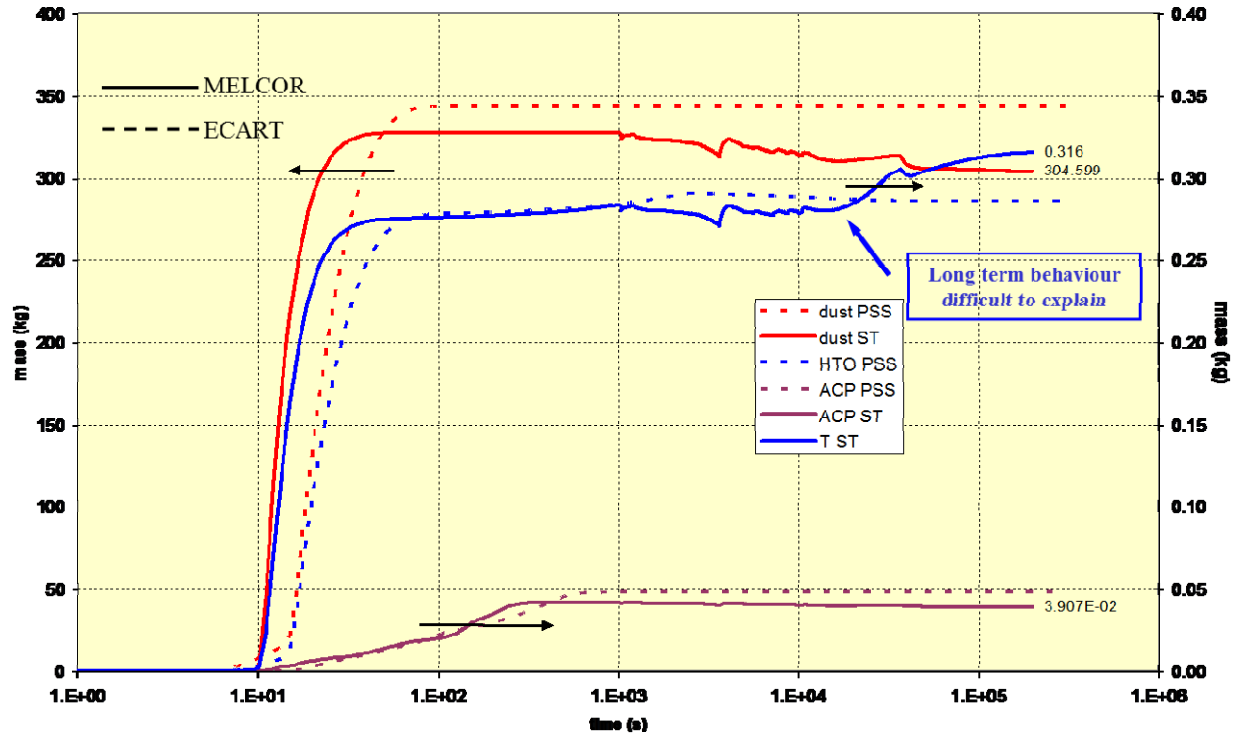

Figure 4.13: Base case – HTO, W and ACP inside the ST.

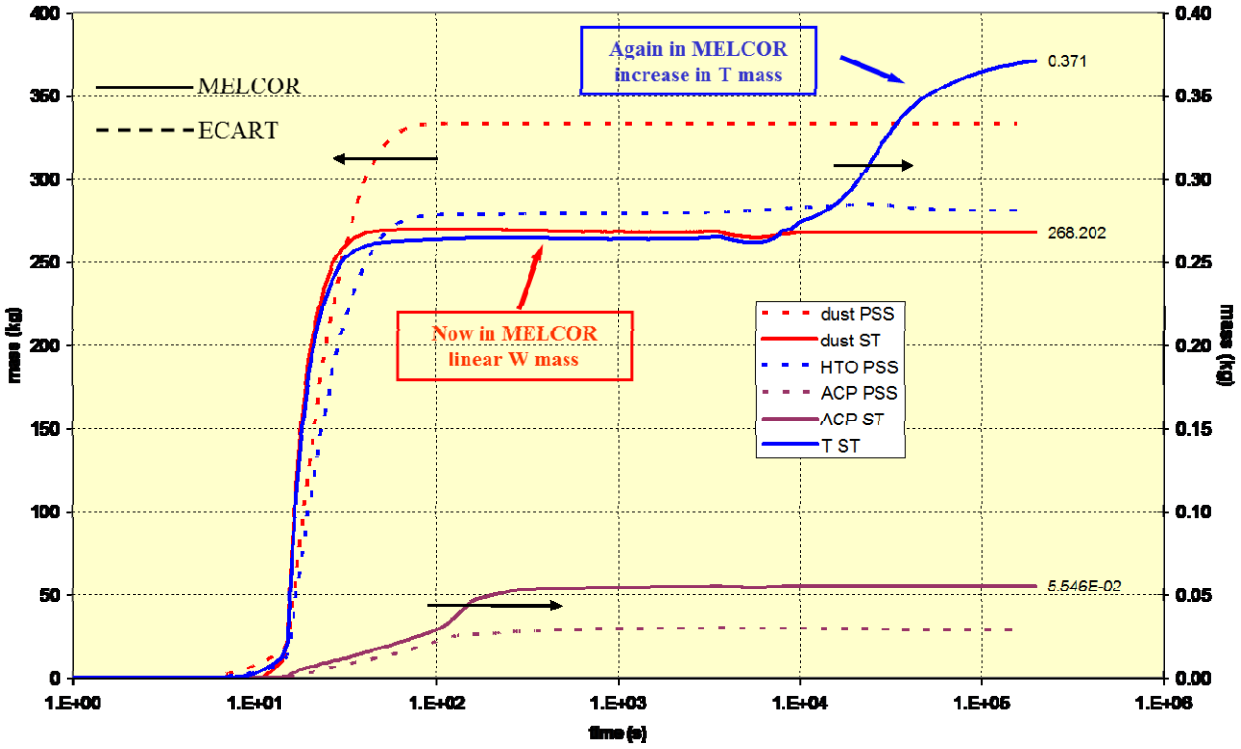

Figure 4.14: Parametric case – HTO, W and ACP inside the ST.

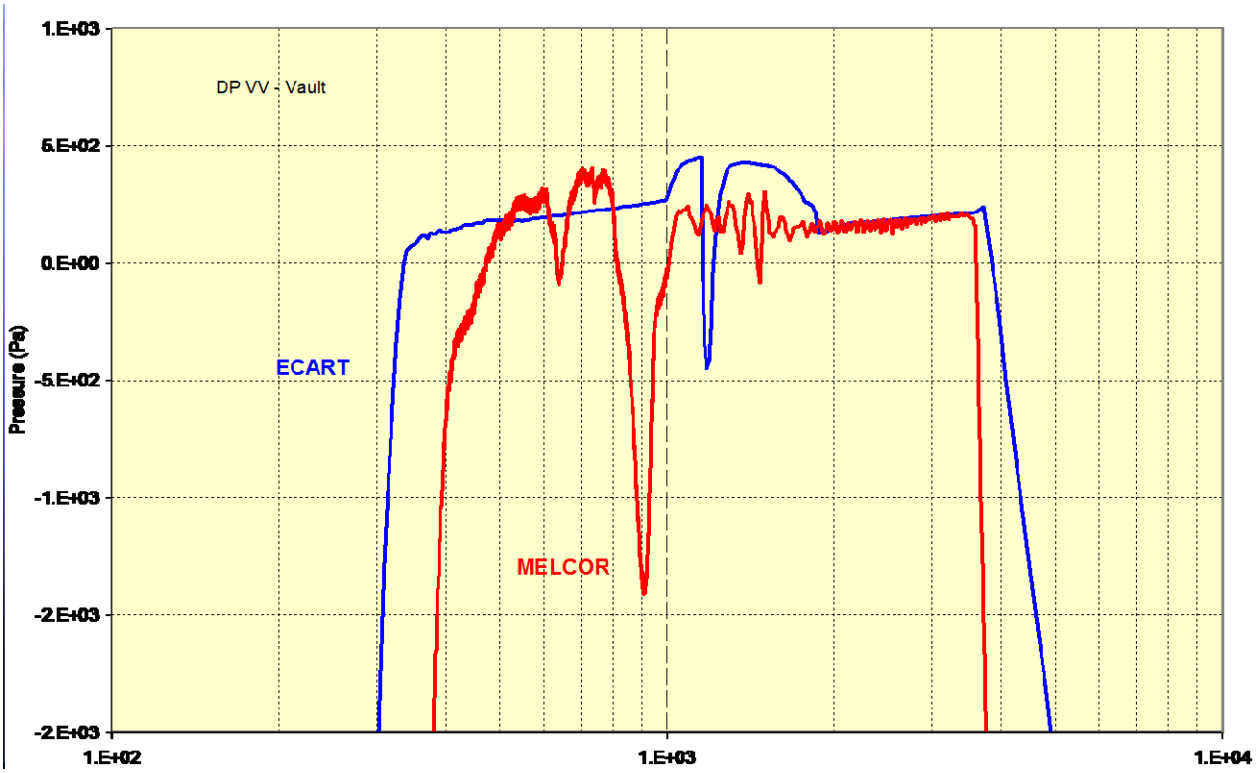

Figure 4.15: Parametric case – Pressure difference between VV and Vault.

4.2.1 External Releases Results

The quantities of the external releases of the radioactive materials (tritium, ACP and W dust) to the environment evaluated by the ECART code in the two analyses are given from Figure 4.16 to Figure 4.25.

For an easier comparison with the available MELCOR plot results for these external releases, the filtering capacity of the different systems (S-VDS, ST-VS and HVAC) have been not considered in the following plots, so an accurate quantitative discussion about these releases will be carried out in the final paragraph. No retention factor has been applied for the uncontrolled releases through the leakages, also if some retention phenomena could be possible in particular inside the concrete cracks.

4.2.1.1 HVAC Releases

The HVAC releases are compared respectively in Figure 4.16 for the base case and in Figure 4.17 for the parametric run.

T ECART predicts higher HTO releases respect to the MELCOR data, in particular for the parametric case. This is due to the higher HTO concentrations predicted in the TCWS atmosphere, as previously discussed.

W Obviously, no W release is predicted through HVAC because this system, working for the TCWS Vault only, is stopped at about 70 s in all the analysis, before the W mass transport from VV into the Vault.

ACP A very nice agreement is present between ECART and MELCOR results, confirming the good characterisation of the input data for this substance and the substantial correctness of the aerosol transport models implemented in the two codes.

4.2.1.2 TCWS Vault Leakage

The uncontrolled releases from the TCWS Vault trough the pressure dependent leakage, characterised as reported in Figure 3.10, are compared respectively in Figure 4.18 for the base case and in Figure 4.19 for the parametric run.

T Again the ECART code predicts higher HTO releases respect to the MELCOR data. This is due to the higher HTO concentrations predicted in the TCWS atmosphere, as previously discussed.

W As for the HVAC system, no uncontrolled W release is predicted through the TCWS Vault leakage because the total pressure of this volume is well below the atmospheric one when the starting of the W transport from the VV into the TCWS Vault is possible, as in the parametric ECART run.

ACP A quite good agreement is again present between the ECART and MELCOR results during the transient phase of the ACP releases but ECART stops these releases at a lower value respect to MELCOR; this is due to the slight lower pressure level predicted by the first code inside the TCWS Vault. This under predicted behaviour is very similar for the base and the parametric cases.

4.2.1.3 S-VDS Releases

The releases through the S-VDS system are compared respectively in Figure 4.20 for the base case and in Figure 4.21 for the parametric run.

T Again the ECART code generally predicts higher HTO releases respect to the MELCOR data. This is due to the higher HTO concentrations predicted in the TCWS atmosphere, as previously discussed. However, quite strange is the long term HTO release (but very small) predicted by MELCOR for the base case, when the HTO mass present inside the TCWS Vault is null (Figure 4.12).

W As before, no W release is predicted through the S-VDS system in the base case while, in the parametric ECART run, a small W release is predicted being more relevant the "by-pass" effect.

ACP Again a quite good agreement is present between ECART and MELCOR results during the transient phase of the ACP releases and this behaviour is similar for the base and the parametric cases.

4.2.1.4 ST-VS Releases

For a rational discussion of the different results for the predicted releases through this ST-VS system, a comparison of the pool scrubbing models implemented inside the two codes should be necessary. As a first snapshot of the situation, for the base case reported in Figure 4.22, a higher scrubbing action is predicted by ECART, for the W dust, in high flow conditions (the W dust is immediately mobilised at the beginning of the discharge from the VV into the suppression pool) while a lower scrubbing action is at the contrary predicted in low flow conditions (in the long term phase of the discharge) for HTO and ACP, mobilised inside the VV more slowly respect to the W dust. These considerations are also confirmed in the parametric case (Figure 4.23) for the W and ACP releases while a substantial concordance between the two codes is predicted for the HTO releases (it is unknown the MELCOR modelling of this substance).

From the comparison between the same code results for the two cases (reported respectively in Figure 4.24 for MELCOR and in Figure 4.25 for ECART) is quite evident the large dependence of the scrubbing action from the flow-rate for ECART respect to the smother behaviour of MELCOR, excluding the ACP.

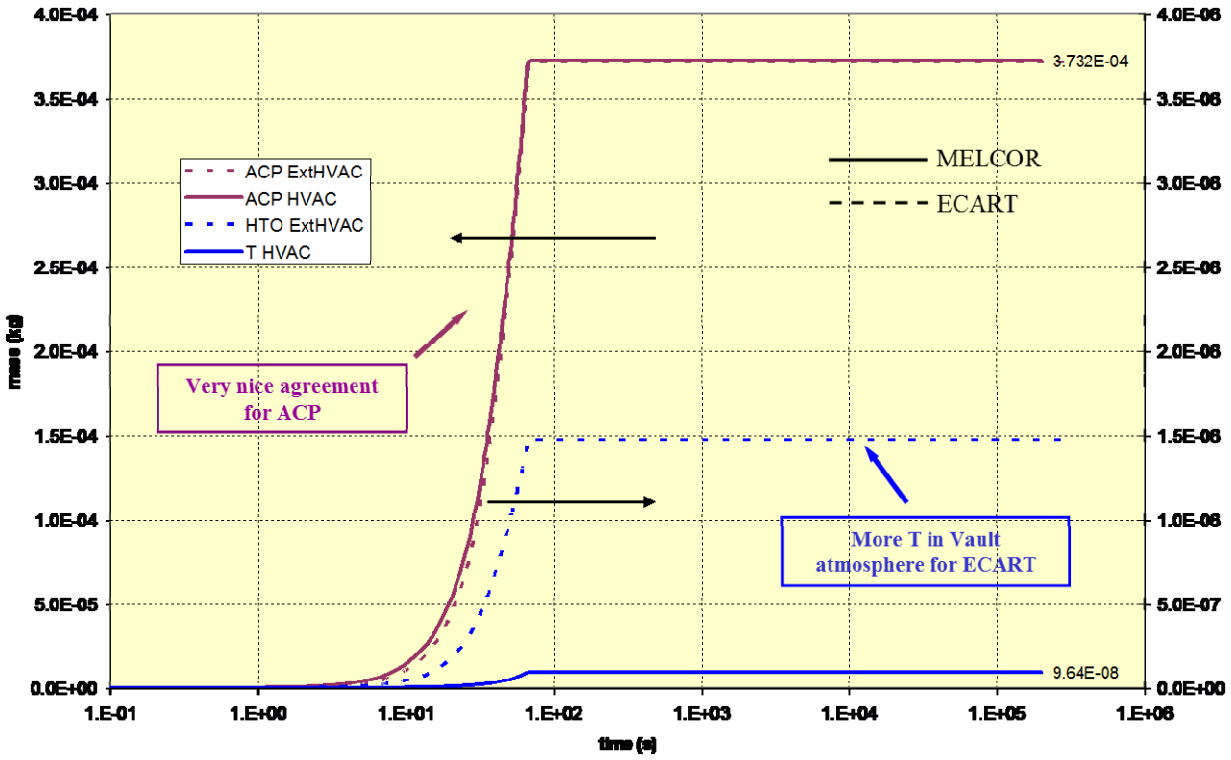

Figure 4.16: Base case – HVAC releases.

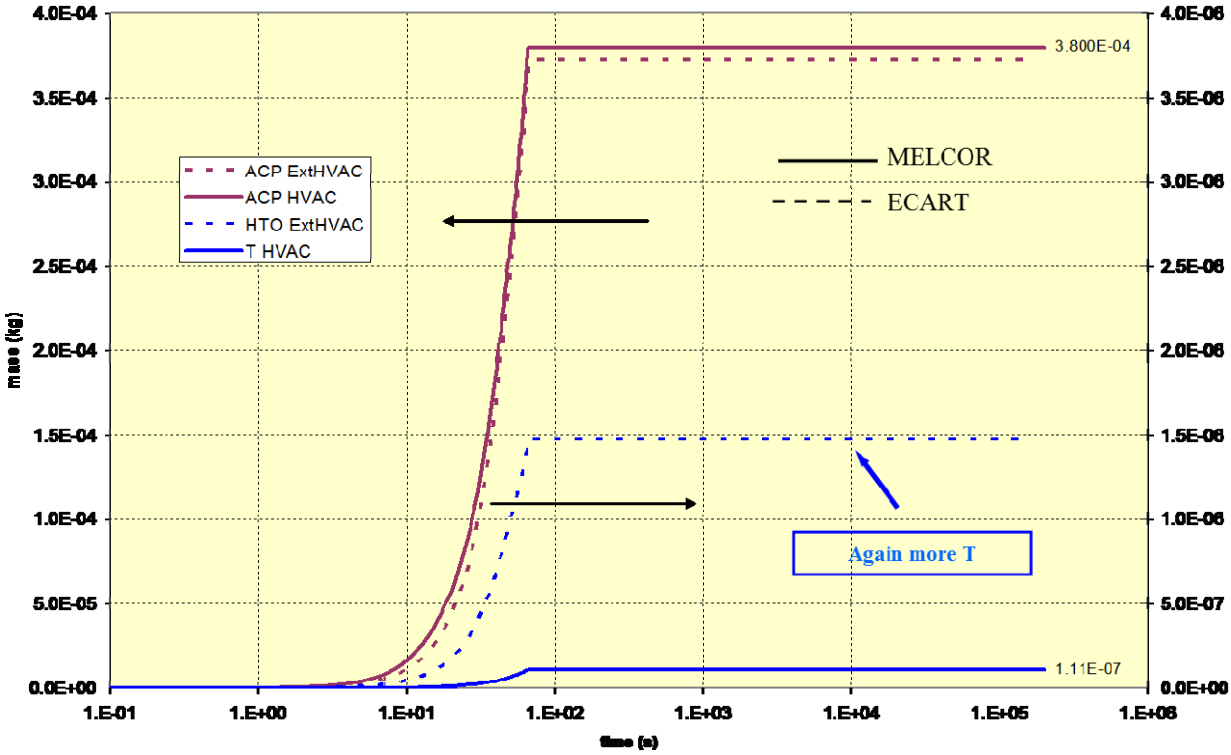

Figure 4.17: Parametric case – HVAC releases.

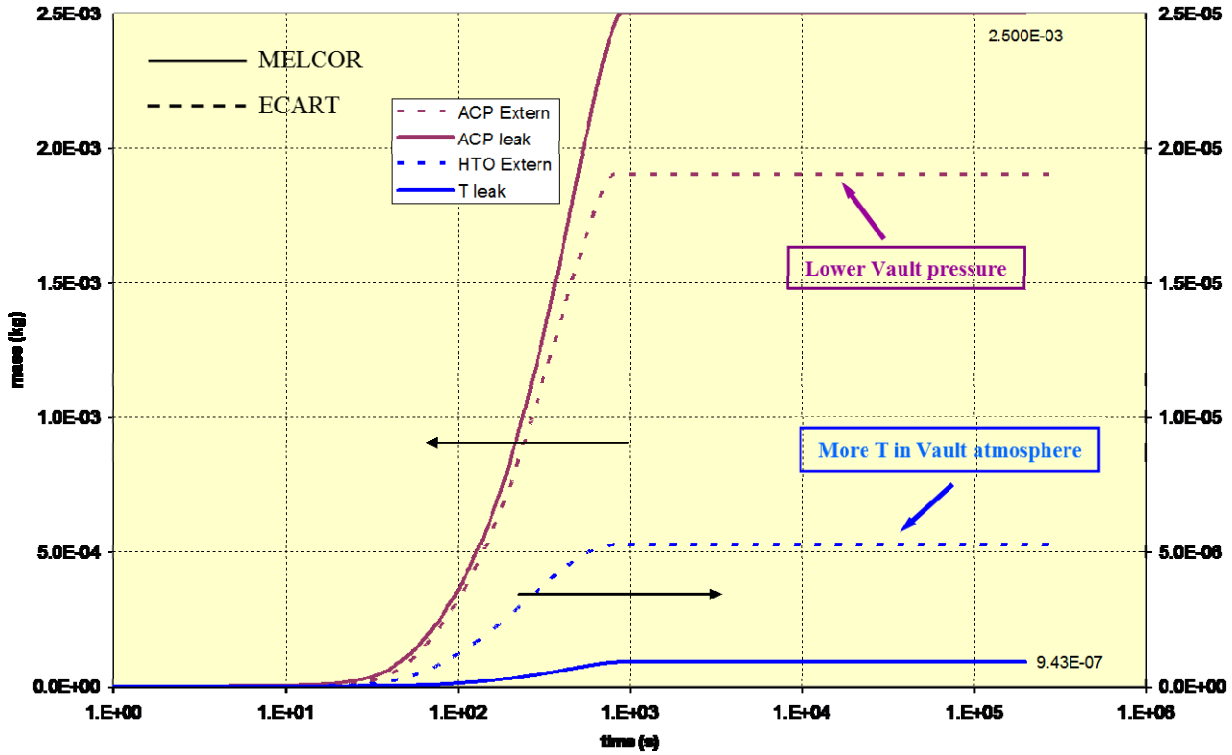

Figure 4.18: Base case – Vault leakage releases.

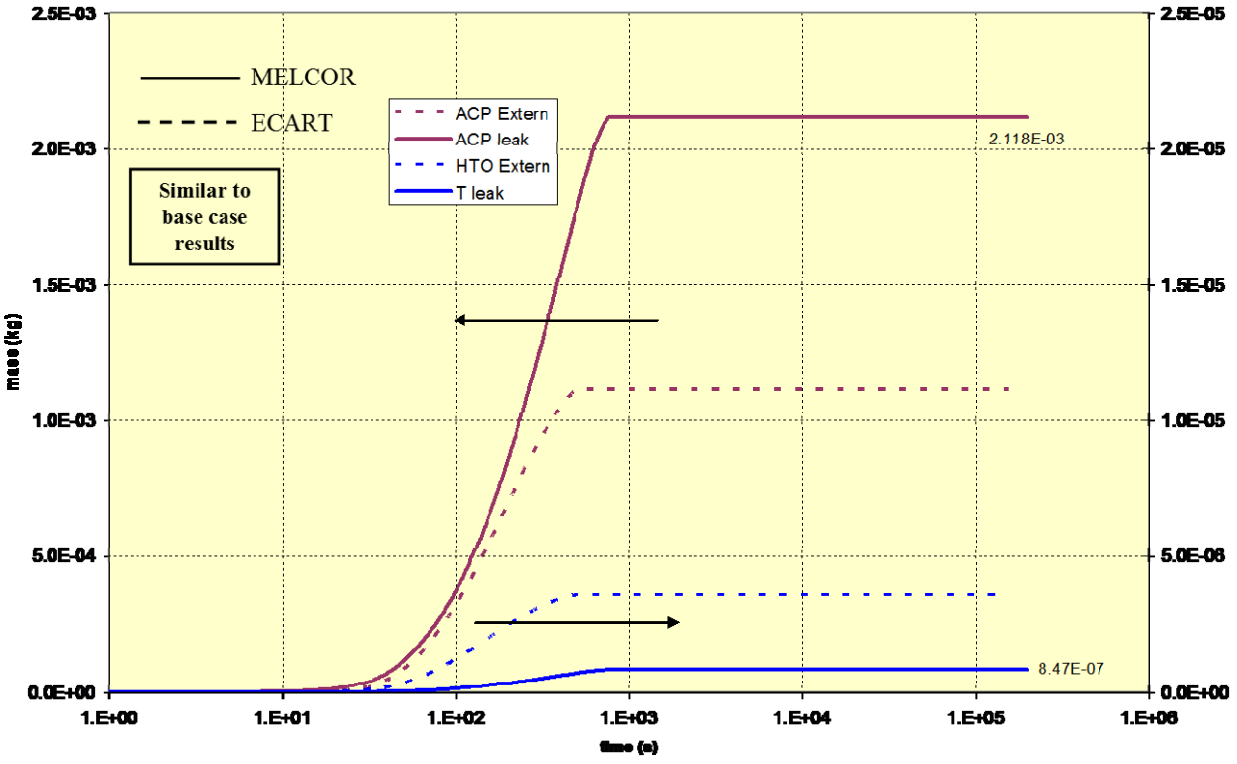

Figure 4.19: Parametric case – Vault leakage releases.

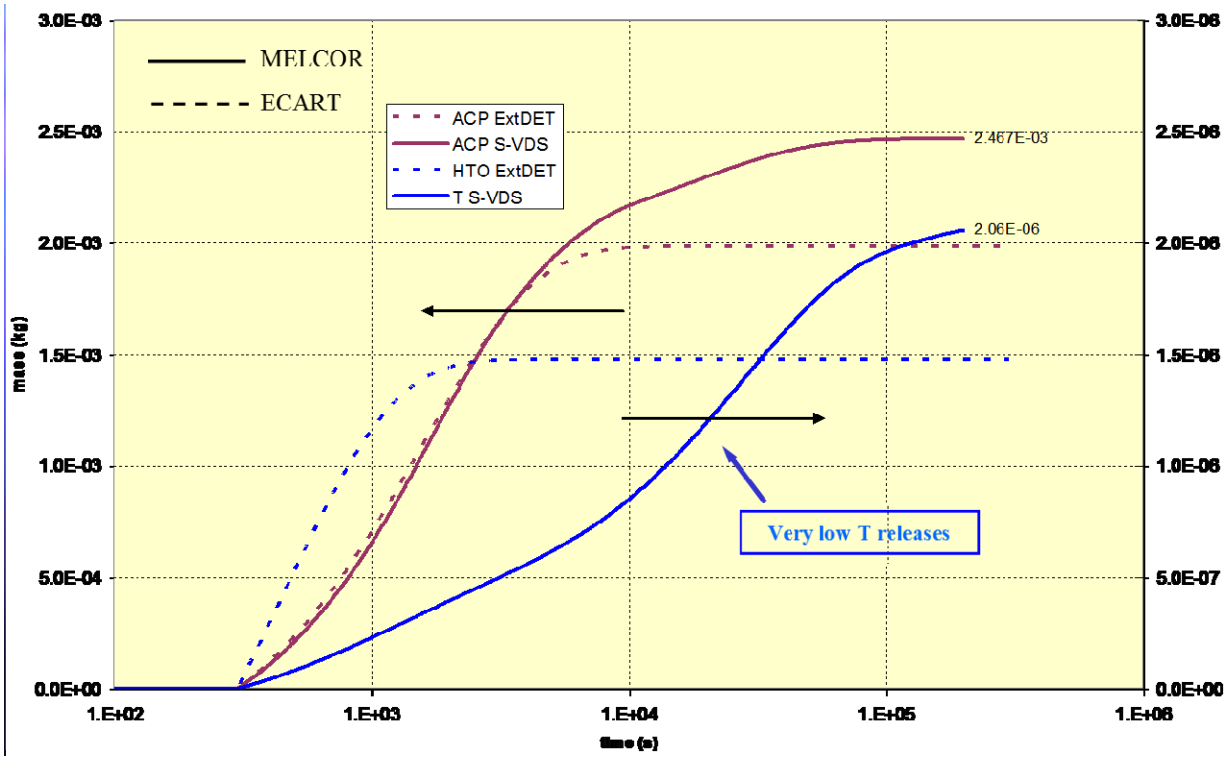

Figure 4.20: Base case – S-VDS releases.

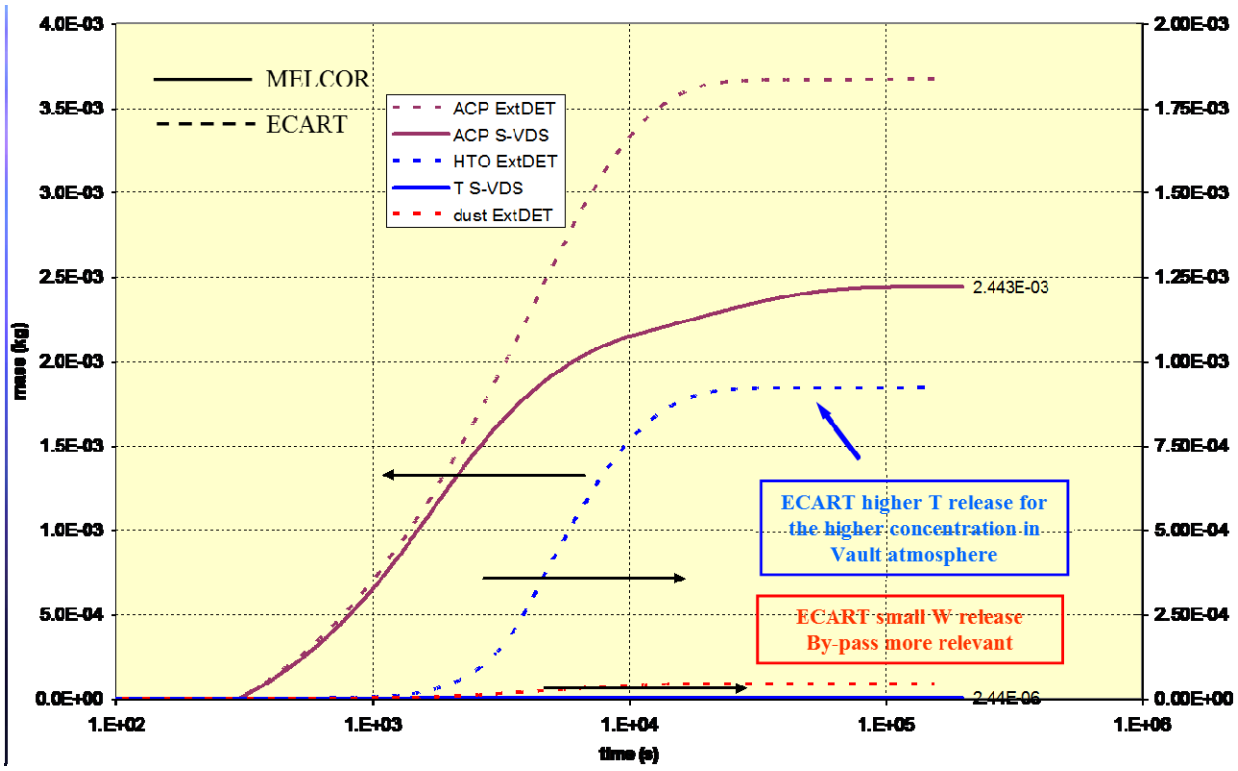

Figure 4.21: Parametric case – S-VDS releases.

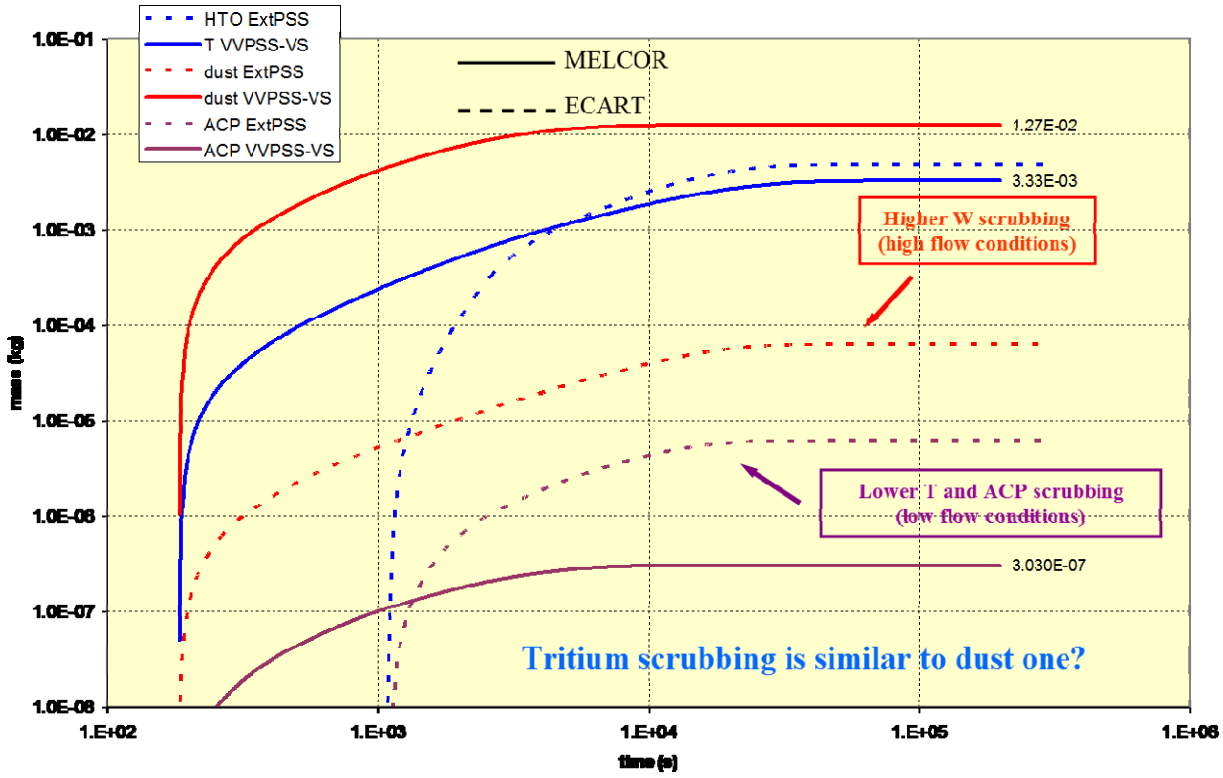

Figure 4.22: Base case – ST-VS releases.

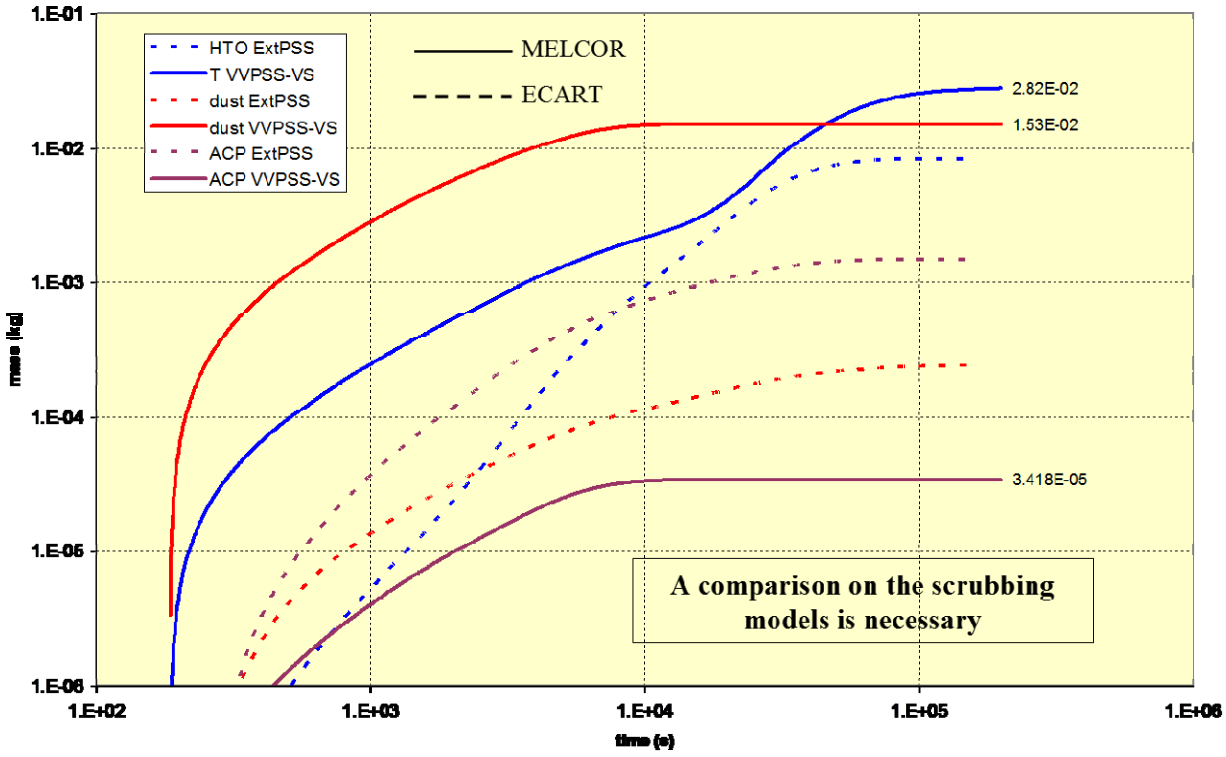

Figure 4.23: Parametric case – ST-VS releases.

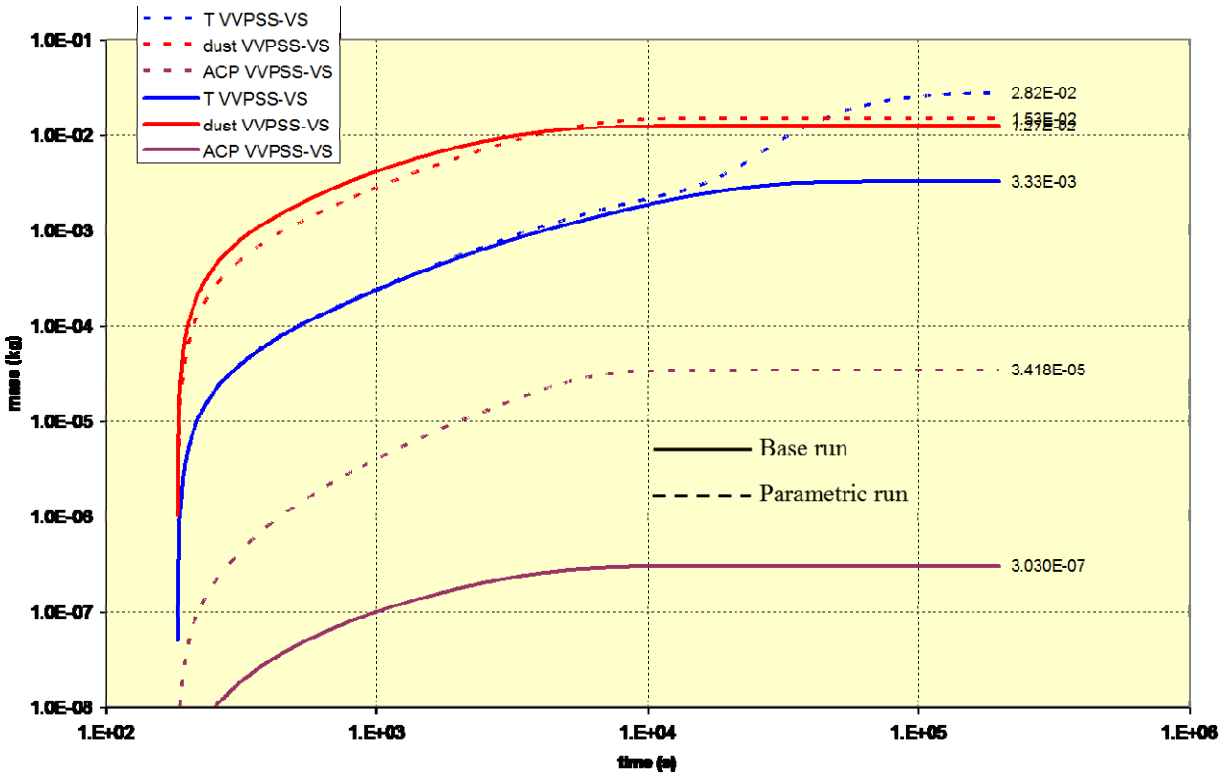

Figure 4.24: MELCOR – ST-VS releases.

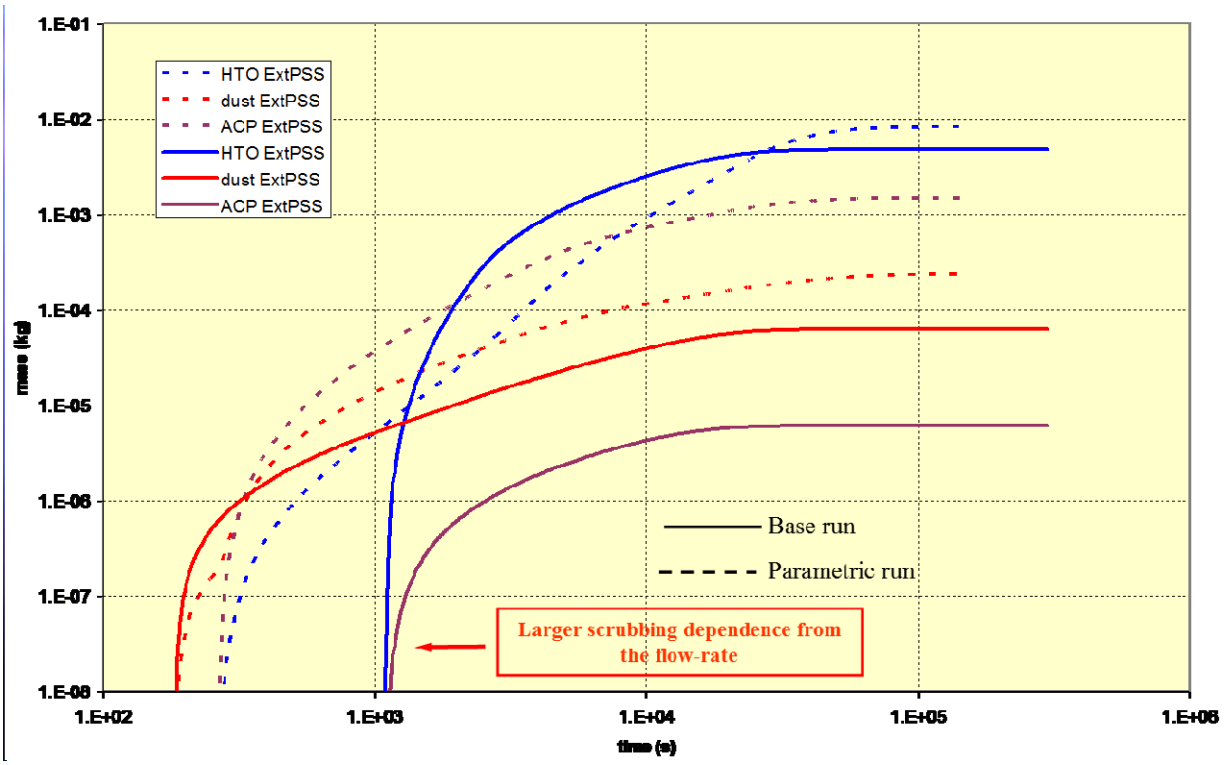

Figure 4.25: ECART – ST-VS releases.

4.2.2 Final Considerations about the External Releases

Some final quantitative considerations about the external releases predicted by ECART are necessary to close the reporting of the analyses, considering that in the previous discussions the filtering capacity (or the removal efficiency) of the different systems (S-VDS, ST-VS and HVAC) have been not considered.

The input assumed removal efficiency of the three systems plus the TCWS Vault leakage for the three different species are reported in the following Table 4.2. It has to be noted that inside SADL [Bartels, 2003 a] the efficiency of the ST-VS for the tritium removal is not directly specified, so it has been assumed equal to the S-VDS one (99 %) on the basis of the Figure 4.26, extracted from the SADL itself [Bartels, 2003 a].

	Leak	ST-VS	S-VDS	HVAC
Tritium	0 %	99 %	99 %	0 %
Dust	0 %	99.9 %	99.9 %	95 %
ACP	0 %	99.9 %	99.9 %	95 %

Table 4.2: Assumed removal efficiency of the different systems.

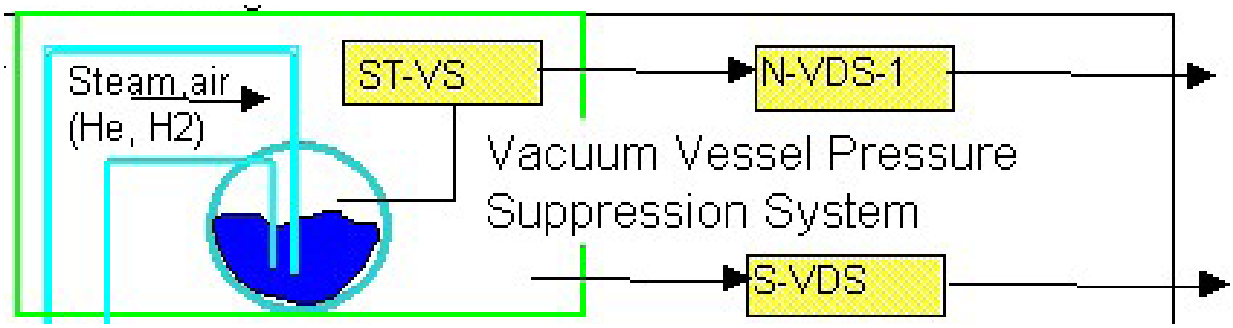

Figure 4.26: Configuration of the ST-VS systems from SADL.

The quantitative summary of the external releases calculated by ECART for the two analyses (the base run and the parametric case) is reported in Figure 4.27 not considering the filtration effects while these effects have been included in the data of Figure 4.28. In each radar plot the following data are reported:

Leak mass releases [kg] trough the TCWS Vault leakages (always unfiltered) of the three species (Tritium, W and ACP);

S-VDS mass releases [kg] trough the S-VDS (filtered or unfiltered) of the three species (Tritium, W and ACP);

ST-VS mass releases [kg] trough the ST-VS (filtered or unfiltered) of the three species (Tritium, W and ACP);

HVAC mass releases [kg] trough the HVAC (filtered or unfiltered) of the three species (Tritium, W and ACP);

Releases total mass [kg] releases (filtered + TCWS Vault leakage) of the three species (Tritium, W and ACP);

Total hypothetical total mass [kg] releases (unfiltered) of the three species (Tritium, W and ACP).

The first Figure 4.27, without considering the removal efficiencies, is significant to understand where the three different species are located inside the ITER plant at the end of the two transients (300,000. s for the base case and about 200,000. s for the parametric run). In particular the following considerations are applicable:

Tritium it is practically pushed all inside the ST-VS for both the analyses, followed by the releases through the TCWS Vault leakage in the base run and through the S-VDS system in the parametric analysis, where it is quite strong the influence of the “by-pass” effect; obviously, no differences are on the contrary present for the HVAC releases, stopped in the initial common part of the accident;

W dust all the external releases of this specie is practically pushed through the ST-VS system, as for the tritium, for both the performed analyses while the S-VDS and the uncontrolled leakage releases are present only in the parametric run, where there is the presence of the “by-pass” effect; no W dust releases are predicted trough the HVAC system, closed in

both the sequences before the W dust incoming from the VV, where it is all mobilised, into the TCWS Vault;

ACP the ACP releases distribution is practically the same for the two analyses with only the increasing of the controlled releases through the ST-VS system for the venting, during all the long term phase of the parametric sequence, of the ACP present inside the TCWS Vault, towards the ST-VS trough the VV.

These qualitative considerations can be transformed in the quantitative (and real) filtered total releases of the ITER plant shown in Figure 4.28 and also reported in Figure 4.29: it is quite clear the increases of the tritium (doubling from about 0.5 mg to about 1 mg) and of the W dust total releases (from about 0.05 mg to about 0.3 mg) in the parametric case (for the increased releases through the S-VDS and the ST-VS systems) and the reduction of the total ACP releases (from about 2 g to about 1 g), for the reduction of the releases through the uncontrolled TCWS Vault leakage, diverted through the filtered ST-VS.

Summarising these results, from the “radar” plots two main points can be highlighted about the total external releases:

a) the tritium and the W dust total releases (the two species initially mobilised inside the VV in relevant quantities) are - above all - due to the contribution of the filtered venting through the ST-VS system;

b) the total ACP releases, driven only by the releases from the coolant into the VV and into the TCWS Vault, are mainly due to the contribution of the uncontrolled leakages from the TCWS Vault.

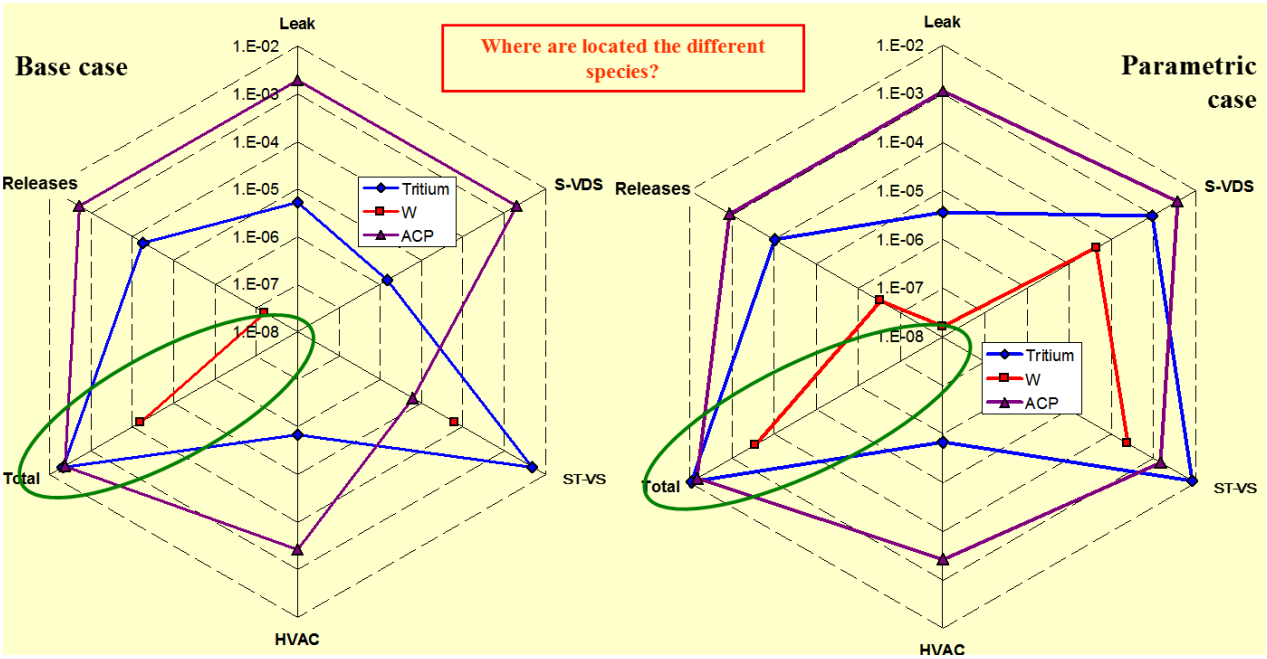

Figure 4.27: Summary of the ECART results for the external releases (unfiltered).

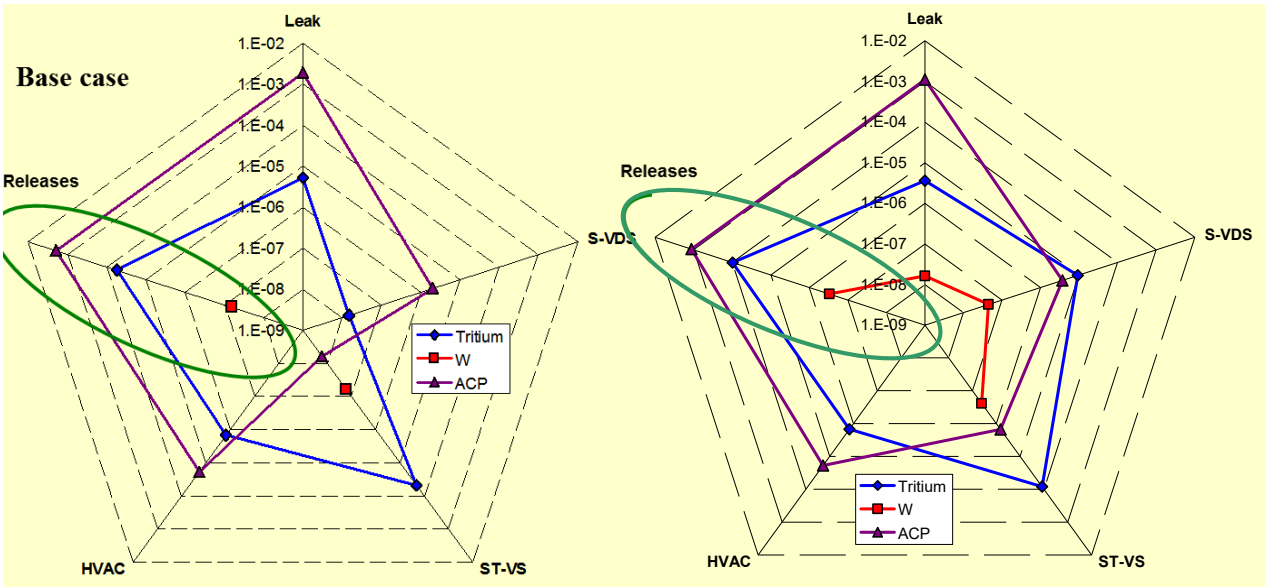

Figure 4.28: Summary of the ECART results for the external releases (filtered).

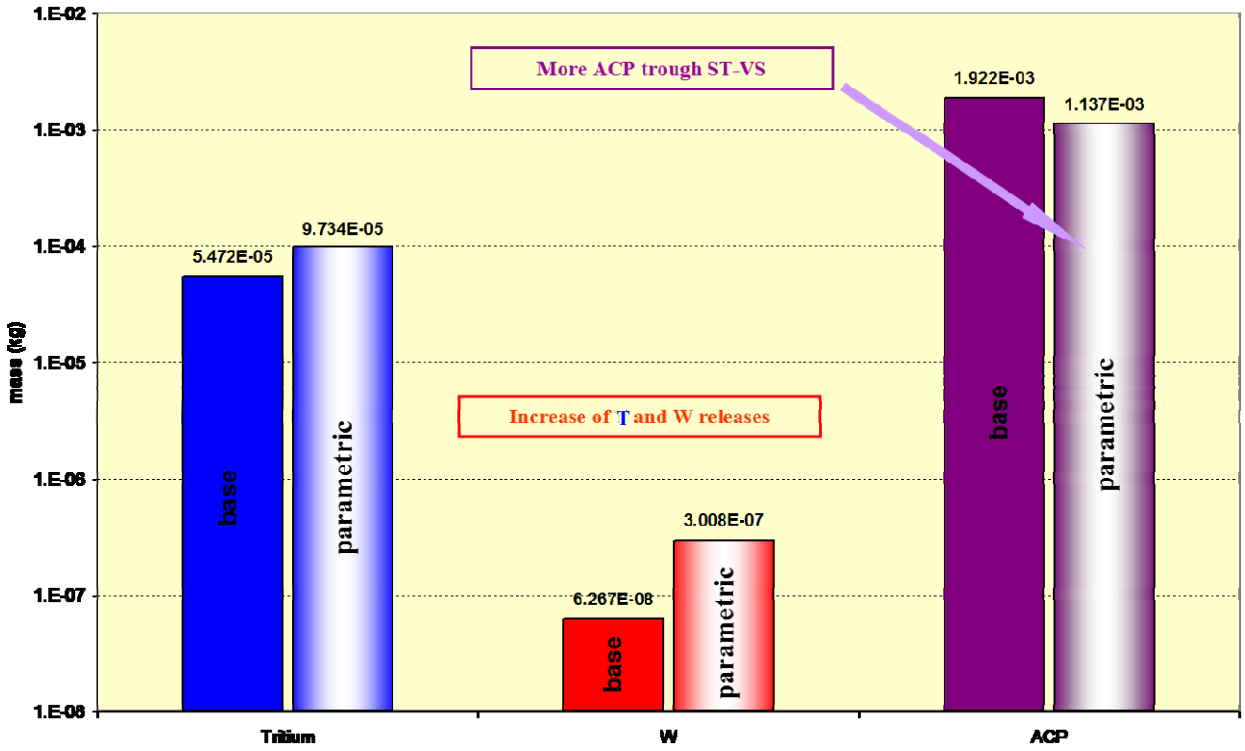

Figure 4.29: Comparison of the ECART results for the external releases.

A final consideration has to be performed, in particular in the case of the W dust: a small external release (ranging from 0.1 to 10.0 g unfiltered) to the outside environment, as predicted by ECART and MELCOR, should be compared to the initial W inventory of 305.0 kg. These very small fractions of the initial inventory are to be considered mainly as an indication of a negligible release to the environment because they are well below the error tolerances associated to the integration methods used to solve the aerosol equations of this family of codes. Furthermore, the uncertainties on the initial and boundary conditions (as the dust granulometry or the tritium characterisation) and on the key parameters characterizing the aerosol models (resuspension fraction inside the VV or in the Vault) make these quantitative comparisons questionable. However, the results obtained with the ECART aerosol models, already tested and validated in the framework of fission reactor studies, can be considered at this stage as indicative of the capacity of the whole system to cope with this relevant accident scenario.

5. Conclusions

The present work represents a significant step in the verification of the ECART capability to treat a typical accident sequence of the ITER plant. The results obtained with its models, already tested and validated in the framework of several fission reactor studies, are promising also in the fusion safety field but, because the inventory released to the external environment is low, to confirm the correctness of the present assessment, future analyses could be addressed to study the transport phenomena in specific circuit parts or components, as the tritium/HTO scrubbing inside the suppression pool, influencing the release itself.

Moreover, as expected, the particles "mobilization" inside the VV just after the break should be further investigated, as it is determinant on the following transport process. Also, it is questionable if the hypothesis of a "*prompt and total*" resuspension could be conservative or not, because an overestimate of the airborne concentration at the first stage of the accident could lead to an overestimation of the particles removal due to the their pushing and the consequent scrubbing inside the suppression tank water. Furthermore, an ad-hoc model for particle scrubbing under the two-phase flow occurring within the cooling circuit at the latest phase of the blow-down could be necessary to better quantify the dust retention within the pipe-work and the fraction of the initial ACP releases from the vaporising coolant escaping from the HTS breaks.

Furthermore, the performed ECART analysis allowed a QA control of the previous MELCOR analyses, and this action has been followed by a revision of the Studsvik MELCOR calculations, giving analyses closer to SADL specifications and confirming, in the same time, the main results about the external consequences predicted by MELCOR.

Concluding, it can be stating that ECART is able to provide a good qualitative & quantitative description of the accident scenario, focused on external releases, also employing a simplified DV circuit nodalisation respect to MELCOR. Mainly, these analyses, form the point of view of ITER safety, confirm that:

a) the accidental overpressure inside the VV and the TWCS Vault is always well below the design limit;

b) the radioactive releases are adequately confined below the ITER guidelines.

About general indications on the preferred flow-paths for the external releases of this ex-vessel break sequence, the following two main conclusions are possible:

a) the tritium and dust total releases are, above all, due to the controlled venting through the ST-VS system;

b) the ACP total releases are mainly due to the uncontrolled leakages from the TCWS Vault.

In deep, from the releases comparison between the two analysed scenarios of this sequence it is possible to highlight as the parametric case, due to the "flow by-pass" occurrence between the VV and the TWCS Vault, mainly causes:

a) an increase of a factor ~2 of the tritium total releases;

b) more relevant total releases for W dust, due to the uncontrolled leakages from the TCWS Vault;

c) lower total releases predicted for the ACP, vented trough the controlled ST-VS system in the opposite of the TCWS Vault uncontrolled leakage dominating the base case ACP total releases.

These ECART analyses, and the comparison with the MELCOR study, have also highlighted some points in the SADL information that will require a more accurate specification to avoid misunderstanding in the future analyses. In particular, the following items have been pointed out as requiring attention by the ITER International Team:

a) characterisation of the tritium releases (as a gas, as a dust – granulometry? - or as HTO vapour?);

b) GSD of the different dusts and ACP initial inventories;

c) real characteristics of the ST-VS system (possible as a characteristic curve function of the ST total pressure) and its removal efficiency.

In particular, relating to this last point, the performed ECART analyses provided further information about the effects of the ST-VS characterisation on the overall thermal-hydraulic transient of the ITER plant and on the subsequent external radioactive releases, highlighting the possible "bifurcation" effect on this thermal-hydraulic transient, also considering uncertainties in the "by-pass" flow determination.

5.1 Future Work and Perspectives

From all the performed analyses some general indications for the *"next step"* code safety analyses are also possible:

a) plot separately the suspended, deposited & pool retained masses of the different species inside the considered control volumes for an easier code comparison;

b) pay attention to the definition of the source term timing, to the tritium form (gas, dust or HTO?) and to the granulometry of the different dusts;

c) pay attention to the ST-VS system characterisation;

d) perform a preliminary comparison of the different models for the "pool scrubbing" phenomenology;

e) further assess the tritium retention inside the scrubbing pool.

Possible tentative specifications of the unclear points for the *"next step"* analysis are reported in the following.

Source Term

- **Hydrogen** production due to the Be-steam reaction modelled as 2.8 kg initially present into the VV (no activation of the code oxidation model to promote the code comparison)

- **Dust** 5 kg mobilised from disruption +
  350 kg immediately mobilized from the in-vessel components
  only W dust taken into account
  (in SADL also dusts formed by Beryllium 100+5 kg and Carbon 200+5 kg)

- **ACP** 10 kg/loop, mobilization 1.3% of the ACP content inside the break mass flow

- **Tritium** concentration of 0.005 g-T/m3 of coolant (total mobilisation in air) +
  1000 g initially present inside the VV
  50% mobilized at disruption, 50% mobilised during the following 6 h
  full mobilisation (vapour)

Physical Status & Granulometry

- Dust — 5 kg: GSD 2.0 – diameter 0.01 micro-m (AMMD)
  350 kg: GSD 2.0 – AMMD 2.11 micro-m
  as suspended aerosol particles
- ACP — GSD 2.0 – AMMD 2.0 micro-m
  as suspended aerosol particles
- Tritium — in-vessel HTO as vapour – liquid aerosol
  in primary water as HTO, possible vaporisation

ST-VS Characterisation

Specifications from SADL		
Feature	**Value**	**Target**
Processing rate	150 m^3-STP/hour	Maintain flow velocity >1 m/s at 0.02 m^2 bypass break

- Constant volumetric flow, simulation using the above reported SADL specifications;
- ST-VS system closed if the total pressure inside the ST is lower than 0.7 Bar;
- No DV valves closure at 3600. s, conservatively to maximise the effects of the “by-pass” flow-rate.

REFERENCES

[Ambrosini, 1995] W. Ambrosini, G. Fruttuoso, F. Oriolo, F. Parozzi, *"Thermal-Hydraulic Modelling in Support to Severe Accident Radionuclide Transport"*, Nuclear Technology, Vol. 112, No. 2, Nov. 1995, pp. 239-249.

[Bartels, 2000] H.W. Bartels, L. Topilski, "*Safety Analysis Data List-3 (SADL-3)",* Report G 81 RI 5 00-02-29, ITER-JCT, February 29, 2000. Section 9, 2000.

[Bartels, 2003 a] H.W. Bartels et al., *"Safety Analysis Data List – 4 (SADL-4) Version 4.0.2"*, ITER JWC, Garching (Germany), August 2003.

[Bartels, 2003 b] *"Accident Analysis Specification (AAS) Version 4.beta.1"*, ITER JWC, Garching (Germany), August 2003.

[Blawzdziewicz, 1995] J. Blawzdziewicz, T.B. Diep, F. Feuillebois, "*Physical Study of Aerosol Transport in the ECART Code",* Report CNRS Laboratoire de Physique et Mécanique des Milieux Hétérogènes - École Supérieure de Physique et de Chimie Industrielles de la Ville de Paris, prepared for EDF, 1995.

[Borioli, 1992] E. Borioli, F. Parozzi,. "*Computer Models on Fission Product and Aerosol behaviour in the LWR Primary Coolant System",* European Commission DG XII Report 14676 EN, November 1992.

[Brockmann 1985] J.E. Brockmann, "*Range of Possible Dynamic and Collision Shape Factors*", Report SAND84 - 0410, Vol. 2, App. F, February 1985.

[Cambi, 2001] G. Cambi, P. Meloni, M.T. Porfiri, "*Additional Accident Safety Analyses for ITER GSSR: a) Pump seizure in divertor HTS, b) Large DV ex-vessel coolant leak",* FUS TN SA-SE-R 08A, May 2001.

[Cambi, 2003] G. Cambi, S. Paci, F. Parozzi, M.T. Porfiri, *"Ex-Vessel Break in ITER Divertor Cooling Loop Analysis with the ECART Code"*, Fusion Engineering and Design, ISSN 0920-3796, Volume 69, Issue 1 – 4, September 2003.

[Forgione, 2004] N. Forgione, S. Paci, F. Parozzi, M.T Porfiri, *"Bases for Dust Mobilisation Modelling in the Light of STARDUST Experiments"*, 3rd International Symposium on "Two-Phase Flow Modelling and Experimentation", Pisa (I), 22 - 24 September 2004.

[GSSR, 2001] *ITER Generic Site Safety Report – Volume VII: Analysis of Reference Events*, ITER-JCT Report, ITER G 84 RI 6 01-07-10 R1.0, July 2001.

[Hervouet, 1995] C. Hervouet, W. Ranval, M. Eusebi, F. Parozzi, "*Fission Product Transport in RCS - Aerosol/Vapour Transport. Part I - Comparison between MAAP and ECART Predictions of Radionuclide Transport throughout a Typical PWR RCS*", ENEL-ATN Final Report for CEC RCA Source Term Project ST(95)-P234, June 1995.

[Jones, 2001] A.V. Jones, et al., *"Validation of Severe Accident Codes Against PHEBUS FP for Plant Applications (PHEBEN2)"*, FISA 2001 Meeting on EU Severe Accident Researches, Luxemburg, 12 - 14 November 2001.

[Oriolo, 1998] F. Oriolo, S. Paci, *"DCMN Calculations for the ICE facility"*, Atti del Dipartimento di Costruzioni Meccaniche e Nucleari, DCMN 016 (98).

[Paci, 2000] S. Paci, *"DIMNP Pre-Test Calculations for the EVITA Facility Using the ECART Code"*, Atti del Dipartimento di Ingegneria Meccanica, Nucleare e della Produzione, DIMNP 017 (00).

[Paci, 2004 a] S. Paci, M.T. Porfiri, *"Post Test Analysis of the Experiments P1-P8 in the ICE Facility Using the ECART Code"*, EFDA Task TW3-TSS-SEA5.5, ENEA FUS Report FUS-TN-SA-SE-R-100, Frascati (RM), February 2004.

[Paci, 2004 b] S. Paci. F. Parozzi, M.T Porfiri, *"Validation of the ECART Code for the Safety Analysis of Fusion Reactors"*, 23rd Symposium on Fusion Technology SOFT 23, Venice (I), 20 – 24 September 2004.

[Paci, 2004 c] S. Paci, N. Forgione, F. Parozzi, M.T Porfiri, *"Bases for Dust Mobilisation Modelling in the Light of STARDUST Experiments"*, 3rd International Symposium on "Two-Phase Flow Modelling and Experimentation", Pisa (I), 22 - 24 September 2004.

[Parozzi, 1991] F. Parozzi, "*The Vapour and Aerosol Transport Module in ECART Code"* European Aerosol Conference, Karlsruhe (D), 16-20 September 1991, J. of Aerosol Science, vol. 22 Suppl. 1, S751, Pergamon Press, 1991.

[Parozzi, 1995] F. Parozzi, T. Albiol, A. Alonso, N. Kourti, P. Merker, D.A. Williams, "*Fission Product Transport in the Reactor Coolant System*", FISA-95 Symposium EU Research on SAs, Luxembourg, 20-22 November 1995.

[Parozzi, 2000] F. Parozzi, R. Fontana, E. Salina, "*New ECART models for analysis of accident scenarios in nuclear fusion reactors",* CESI Report n.53/ST-CO-04.03.99, April 2000.

[Sheng, 2003] C.H. Sheng, L.L. Sponton , *"ITER Divertor Ex-vessel Pipe Break"*, N(R)-03/075 Studsvik Nuclear AB, Nyköping (Sweden), December 2003.

[Topilski, 2004] L. Topilski, *"Consequences of large ex-vessel and in-vessel coolant breaks in the divertor cooling loop with different models of air bypass"*, G 84 RI 23 04-06-15 R 0.1 June 15, 2004.

[Wright, 1994] A.L. Wright, *"Primary System Fission Product Release and Transport: a State of the Art Report to the CSNI"*, NUREG/CR-6193, NEA/CSNI/R(94), June 1994.